AD-A104 172 SYRACUSE UNIV NY F/G 11/4
ELECTROMAGNETIC SHIELDING EFFECTIVENESS FOR ISOTROPIC AND ANISO--ETC(U)
JUN 81 J L ALLEN F30602-79-C-0011
UNCLASSIFIED RADC-TR-81-162 NL

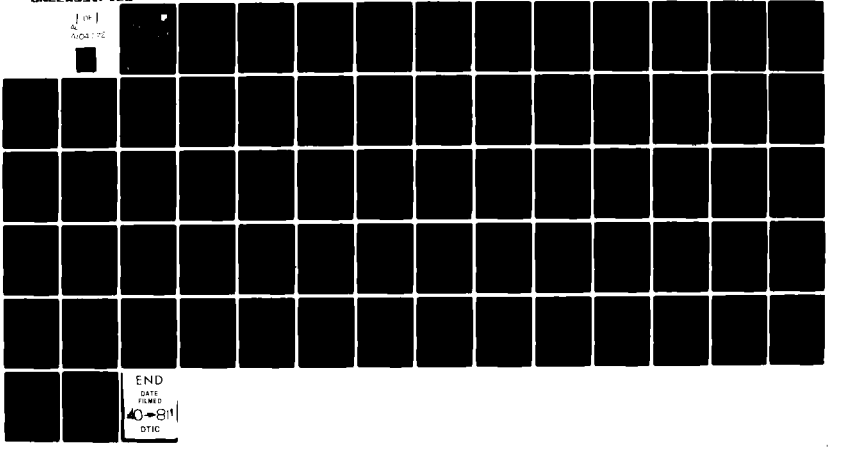

END
DATE FILMED
10-81
DTIC

RADC-TR-81-162
Phase Report
June 1981

ELECTROMAGNETIC SHIELDING EFFECTIVENESS FOR ISOTROPIC AND ANISOTROPIC MATERIALS

Syracuse University

J. L. Allen

ROME AIR DEVELOPMENT CENTER
Air Force Systems Command
Griffiss Air Force Base, New York 13441

This report has been reviewed by the RADC Public Affairs Office (PA) and is releasable to the National Technical Information Service (NTIS). At NTIS it will be releasable to the general public, including foreign nations.

RADC-TR-81-162 has been reviewed and is approved for publication.

APPROVED: Roy F. Stratton

ROY F. STRATTON
Project Engineer

APPROVED: David C. Luke

DAVID C. LUKE, Colonel, USAF
Chief, Reliability & Compatibility Division

FOR THE COMMANDER: John P. Huss

JOHN P. HUSS
Acting Chief, Plans Office

If your address has changed or if you wish to be removed from the RADC mailing list, or if the addressee is no longer employed by your organization, please notify RADC (RBCT) Griffiss AFB NY 13441. This will assist us in maintaining a current mailing list.

Do not return this copy. Retain or destroy.

UNCLASSIFIED

SECURITY CLASSIFICATION OF THIS PAGE (When Data Entered)

REPORT DOCUMENTATION PAGE	READ INSTRUCTIONS BEFORE COMPLETING FORM
1. REPORT NUMBER: RADC-TR-81-162	2. GOVT ACCESSION NO.: AD-A104 172	3. RECIPIENT'S CATALOG NUMBER
4. TITLE (and Subtitle): ELECTROMAGNETIC SHIELDING EFFECTIVENESS FOR ISOTROPIC AND ANISOTROPIC MATERIALS	5. TYPE OF REPORT & PERIOD COVERED: Phase Report. Nov 78 – Mar 80
	6. PERFORMING ORG. REPORT NUMBER: N/A
7. AUTHOR(s): J. L. Allen *	8. CONTRACT OR GRANT NUMBER(s): F30602-79-C-0011
9. PERFORMING ORGANIZATION NAME AND ADDRESS: Syracuse University, Syracuse NY 13210	10. PROGRAM ELEMENT, PROJECT, TASK AREA & WORK UNIT NUMBERS: 62702F, 23380317
11. CONTROLLING OFFICE NAME AND ADDRESS: Rome Air Development Center (RBCT), Griffiss AFB NY 13441	12. REPORT DATE: June 1981 13. NUMBER OF PAGES: 72
14. MONITORING AGENCY NAME & ADDRESS(if different from Controlling Office): Same	15. SECURITY CLASS. (of this report): UNCLASSIFIED 15a. DECLASSIFICATION DOWNGRADING SCHEDULE: N/A

16. DISTRIBUTION STATEMENT (of this Report)

Approved for public release; distribution unlimited.

17. DISTRIBUTION STATEMENT (of the abstract entered in Block 20, if different from Report)

Same

18. SUPPLEMENTARY NOTES

RADC Project Engineer: Roy F. Stratton (RBCT)

* J. L. Allen, University of South Florida, Tampa FL 33620

19. KEY WORDS (Continue on reverse side if necessary and identify by block number)

Electromagnetic Compatibility
Shielding Effectiveness
Anisotropic Fiber
Reinforced Plastic
Scattering Parameters

20. ABSTRACT (Continue on reverse side if necessary and identify by block number)

"ABCD" and "Scattering" matrix analysis techniques for determining shielding effectiveness of isotropic and anisotropic multilayered shields are presented. These techniques are well-suited to computer implementation. A variety of materials fit the models used including advanced composite materials (e.g., fiber-reinforced epoxies where the fibers are "long" and "oriented"), conductive filled thermoplastics (randomly oriented, chopped fibers or other conductive particles) and

DD FORM 1 JAN 73 1473 EDITION OF 1 NOV 65 IS OBSOLETE

UNCLASSIFIED

SECURITY CLASSIFICATION OF THIS PAGE (When Data Entered)

the more common metallic shields. Advanced composite materials are now widely used as structural and surface components in aircraft and spacecraft. Chopped-fiber-filled structural foams are used as enclosures for electronic equipment. Such applications require accurate assessment of electromagnetic shielding effectiveness.

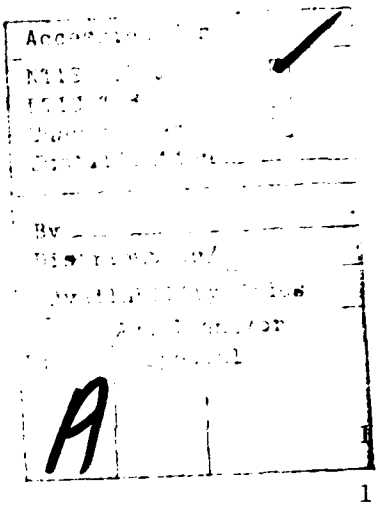

TABLE OF CONTENTS

ELECTROMAGNETIC SHIELDING EFFECTIVENESS FOR ISOTROPIC AND ANISOTROPIC MATERIALS

1. INTRODUCTION

The purpose of this report is to present analysis techniques applicable to the assessment of electromagnetic shielding effectiveness of a variety of types of materials including advanced composite materials (e.g., fiber-reinforced epoxies where the fibers are "long" and "oriented"), conductive filled thermoplastics (randomly oriented, chopped fibers or other conductive particles) and the usual metallic shields. Advanced composite materials are now widely used as structural and surface components in aircraft and spacecraft. Chopped-fiber-filled structural foams are used as enclosures for electronic equipment. Such applications require accurate assessment of electromagnetic shielding effectiveness.

The following sections present a unified approach to plane-wave shielding analysis using ABCD and scattering parameter techniques based on analogies with distributed networks. Related techniques and preliminary results were presented in an earlier report [1]. Some key results from [1] are included in this report for completeness.

Chapters 2 and 3 present background material. Several important results for isotropic materials are developed in Chapter 3 and presented in new formats. Chapter 4 introduces scattering parameter techniques. Chapter 5 treats anisotropic multilayered shields from several points of view, including a very general arbitrary polarization, arbitrary angle of incidence analysis.

2. BACKGROUND

An electromagnetic shield is an enclosure intended to prevent electromagnetic energy within it from escaping and conversely to prevent electromagnetic energy exterior to it from penetrating to the interior. A perfect shield would provide total isolation between interior and exterior. In practice the degree of isolation between interior and exterior is less than perfect and seldom exceeds 100 dB.

The degree of isolation provided between interior and exterior of a shield is commonly called its shielding effectiveness. A measure of shielding effectiveness could be obtained by determining field strength at a particular location inside the shield and then removing the shield and determining the ambient field strength. Errors can occur in such measurements due to such effects as modification of the sources of the external ambient field by the presence of the shield, and proximity effects on the internal field measuring device caused by the shield walls.

Shielding effectiveness is, thus, the insertion loss incurred by electromagnetic energy in passing from an input medium through a shield into an output medium. Both reflection and absorption contribute to shielding effectiveness. Aircraft require substantial electromagnetic shielding to protect sensitive internal electronics from extraneous signals. Some vital areas particularly sensitive to inadequate shielding include low-level integrated

circuit communication and navigation equipment, fly-by-wire systems, fire control systems, and electro-explosive devices.

In a typical situation the skin of an aircraft might be considered the shield with the air external to the vehicle as the input medium and a complex mixture of personnel, air, cables, electronic devices, fittings, etc. of the aircraft's interior as the output region. The external electromagnetic field to be excluded from the interior of the shield might be produced by any of a variety of electromagnetic sources including a direct lightning strike to the aircraft, a nearby lightning strike, a nearby radar or other high-powered transmitter, or perhaps by a nuclear detonation (EMP). Alternatively, the shield may be the cabinet enclosure of an on-board piece of equipment whose interior is to be protected from all the above types of signals plus possible interference from other on-board equipment.

Potential interfering electromagnetic fields may arise from "nearby" or "distant" generating sources. "Near" to a generating source, usually either the electric or the magnetic component of the field will dominate. For sources that resemble loops of current, magnetic field dominates in the region near to the source. For sources that resemble linear dipoles, electric field dominates in the region near to the source. Sufficiently far from either type of source, the propagating field becomes a plane wave in which the field energy is equally divided between the magnetic and electric field components.

Wave impedance is defined as a ratio of electric to magnetic field components. For a plane wave that ratio is 120π ohms or approximately 377 ohms. Near to current loop type sources the wave impedance is very small compared to 377 ohms because the magnetic field is large relative to the electric field. Near to linear dipole type sources the wave impedance is very high compared to 377 ohms because the electric field is large relative to the magnetic field. Wave impedance of the energy incident on a shield is a critical factor in determining whether or not the shield will be effective in excluding the signal. It turns out (as will be seen) that it is much more difficult to shield "low-impedance" magnetic-type waves than to shield either "high-impedance" electric-type waves or "normal-impedance" plane waves. Shielding against low-impedance waves is particularly difficult at low frequencies.

A rough guideline for separating sources into "nearby" and "distant" types is to consider it a nearby source if it is closer than one-tenth of a wavelength to the shield. At 100 KHz, 1 MHz, 100 MHz, and 1 GHz one-tenth wavelength is approximately 1000 feet, 100 feet, 1 foot and 0.1 feet, respectively. Thus, for frequencies up to about 1 GHz, one-tenth wavelength is a relatively large distance compared to the size of modern circuits and "near fields," at least from other on-board equipment, may cut across several circuits.

Practical shields seldom have shielding effectivenss greater than 100 dB. Metals are in general good electromagnetic shields. Shielding effectiveness of a metal structure is degraded by the presence of fabrication seams and joints, access doors and windows and other apertures. A metal aircraft with the usual apertures seams and cracks will have an effective overall shielding of the order of 20 dB at UHF frequencies. Commonly used composite materials,

composed typically of small, relatively poorly conducting fibers embedded in an insulating matrix, provide considerably less shielding particularly at lower frequencies. Metal matrix composites and insuiating matrix composites with metallic fibers are being studied, and from the point of view of electromagnetic shielding such materials would clearly be superior.

3. SHIELDING THEORY

Shielding effectiveness (S.E.) is an exceptionally difficult quantity to evaluate for a given material because S.E. dpends not only on intrinsic material parameters but also is a strong function of shield geometry and of both internal and external environments of the shield. In actual situations internal and external shield environments are usually complicated and time varying (e.g., internal-personnel and equipment inside an aircraft; external-aircraft in hanger, on runway, in air). In addition real shields have a variety of seams, joints and apertures that generally degrade shielding effectiveness. Approximations are necessary in order to reduce a shielding configuration to a manageable electromagnetic boundary value problem.

Plane wave shielding theory has long been used as an aid in characterizing materials and providing a baseline measure of shielding effectiveness. In this report plane wave shielding theory is extended to several classes of anisotropic materials and recast in the very useful scattering parameter format. Coupling mechanisms that degrade instrinsic shielding are briefly described.

3.1 Plane Wave Normally Incident on Infinite Flat Plate

The manner in which an electromagnetic shield transmits plane electromagnetic waves has been shown [2] to be analogous to the manner in which a conventional transmission line transmits electrical current and voltage. An idealized configuration consisting of a plane wave normally incident on an infinite flat plate shield, as shown in Figure 1, provides a useful baseline or reference value of shielding effectiveness. It also serves as a surprisingly good approximate model for a number of more complex configurations that are used for laboratory evaluation of shielding effectiveness. As a first step it is assumed that the shield material is homogeneous and is isotropic in the plane of the shield. This hypothesis obviously includes the usual metallic shields but it also appears to include multilayer graphite epoxy laminates in which the layers are oriented at different angles (e.g., 0°-90°-0°). Unidirectional laminates and perhaps even multilayer, mixed orientation boron laminates require a different hypothesis taking into account the three-dimensional anisotropy effects. The less complex behavior of the multilayer, mixed-orientation graphite laminates arises from the fiber-to-fiber contact between layers. The more complex unidirectional layer configuration has also been modelled and is discussed in Section 5.3 of this report.

Using the well known transmission-line analogy [2] of plane wave propagation as shown schematically in Figure 2, all types of 2-port representations [3] may be utilized to represent the shield. The "Z" and "ABCD" parameter representations have been widely and successfully used in the past. Scattering ("S") parameters [4] offer in many instances distinct advantages such as ease

of automated measurement and direct interpretation in terms of transmitted and reflected components. Scattering parameters are treated in Chapter 4 and applied to multilayer anisotropic shields in Chapter 5. The scattering parameter approach is equally valid and easy to use for the isotropic, homogeneous shield. However, to facilitate comparison with certain classical results, the immediately following analysis is carried out in terms of ABCD parameters. A simple scheme for conversion to S-parameters is given in Section 4.3. The computer programs used for numerical evaluation of shielding effectiveness use a combination of multiport ABCD and scattering parameters.

Figure 3 (a-c) illustrates the details of the schematic representation of plane wave propagation via the transmission-line analogy. Proper choice of the source and load wave impedances (Z_{ws} and Z_{wL}) permit this model to be used even when the incident wave is not a plane wave, e.g., in the near field of a loop of current. This technique is illustrated for a two-loop measurement configuration in Section 3.2. The basic procedure is to analyze the transmission line model to determine its total insertion loss. That insertion loss is then the same as the shielding effectiveness of the shield modelled.

The overall ABCD matrix for the shield with the effects of the output medium included is obtained as the product of the matrices for the individual components and is given by:

$$\begin{bmatrix} A_T & B_T \\ C_T & D_T \end{bmatrix} = \begin{bmatrix} \tilde{A} & \tilde{B} \\ \tilde{C} & \tilde{D} \end{bmatrix} \begin{bmatrix} 1 & 0 \\ \frac{1}{Z_{wL}} & 1 \end{bmatrix} = \begin{bmatrix} (\tilde{A} + \frac{\tilde{B}}{Z_{wL}}) & \tilde{B} \\ (\tilde{C} + \frac{\tilde{D}}{Z_{wL}}) & \tilde{D} \end{bmatrix} \tag{1}$$

where $\tilde{A} = \tilde{D} = \cosh\theta$

$\tilde{B} = \eta \sinh\theta$

$\tilde{C} = 1/\eta \sinh\theta$

and

$\eta = \sqrt{\mu/\varepsilon}$ = intrinsic wave impedance

$\theta = \gamma t$ = electrical length

γ = propagation factor

μ = permeability

ε = permittivity.

Thus,

$$\begin{bmatrix} V_1 \\ I_1 \end{bmatrix} = \begin{bmatrix} A_T & B_T \\ C_T & D_T \end{bmatrix} \begin{bmatrix} V_L \\ -I_L \end{bmatrix} \text{ where } I_L = 0. \tag{2}$$

$$V_1 = V_1^i + V_1^r = V_1^i(1 + \rho_{in}) \tag{3}$$

$$I_1 = I_1^i + I_1^r = \frac{V_1^i}{Z_{ws}}(1 - \rho_{in})$$

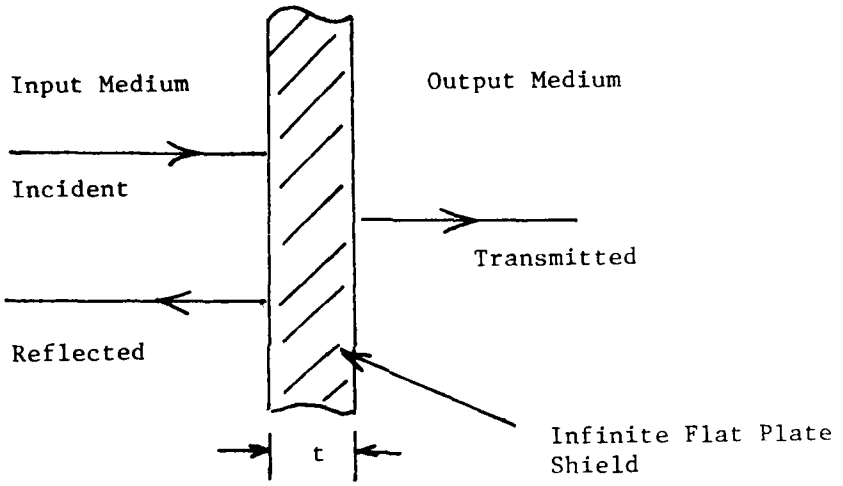

$$\text{Shielding (dB)} = 10 \log_{10}\left(\frac{\text{Transmitted Power}}{\text{Incident Power}}\right)$$

Figure 1. Plane Wave Shielding

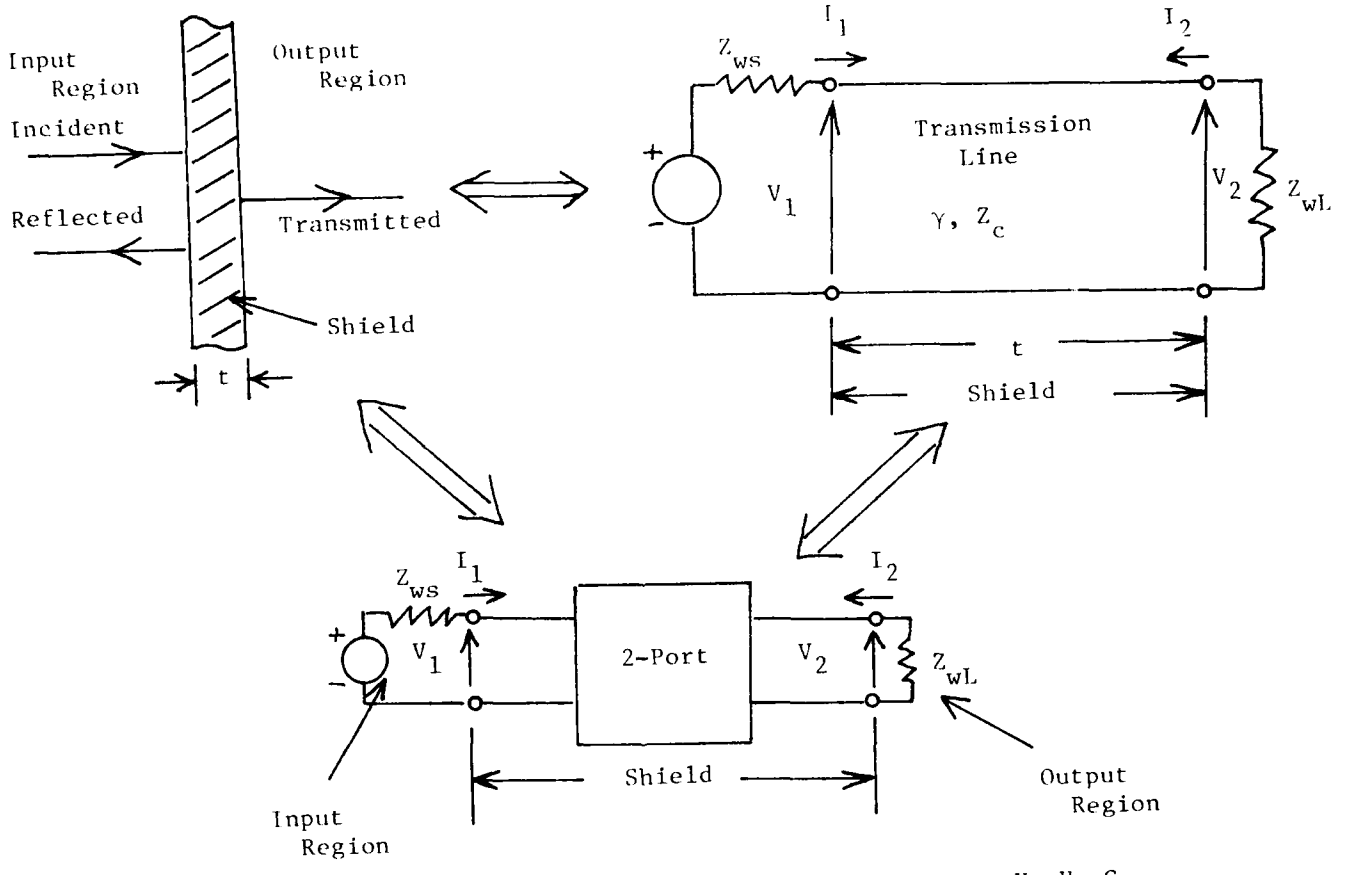

Figure 2. Schematic Representation of 2-Port for Z, Y, H, G, "ABCD," or S Parameter Description.

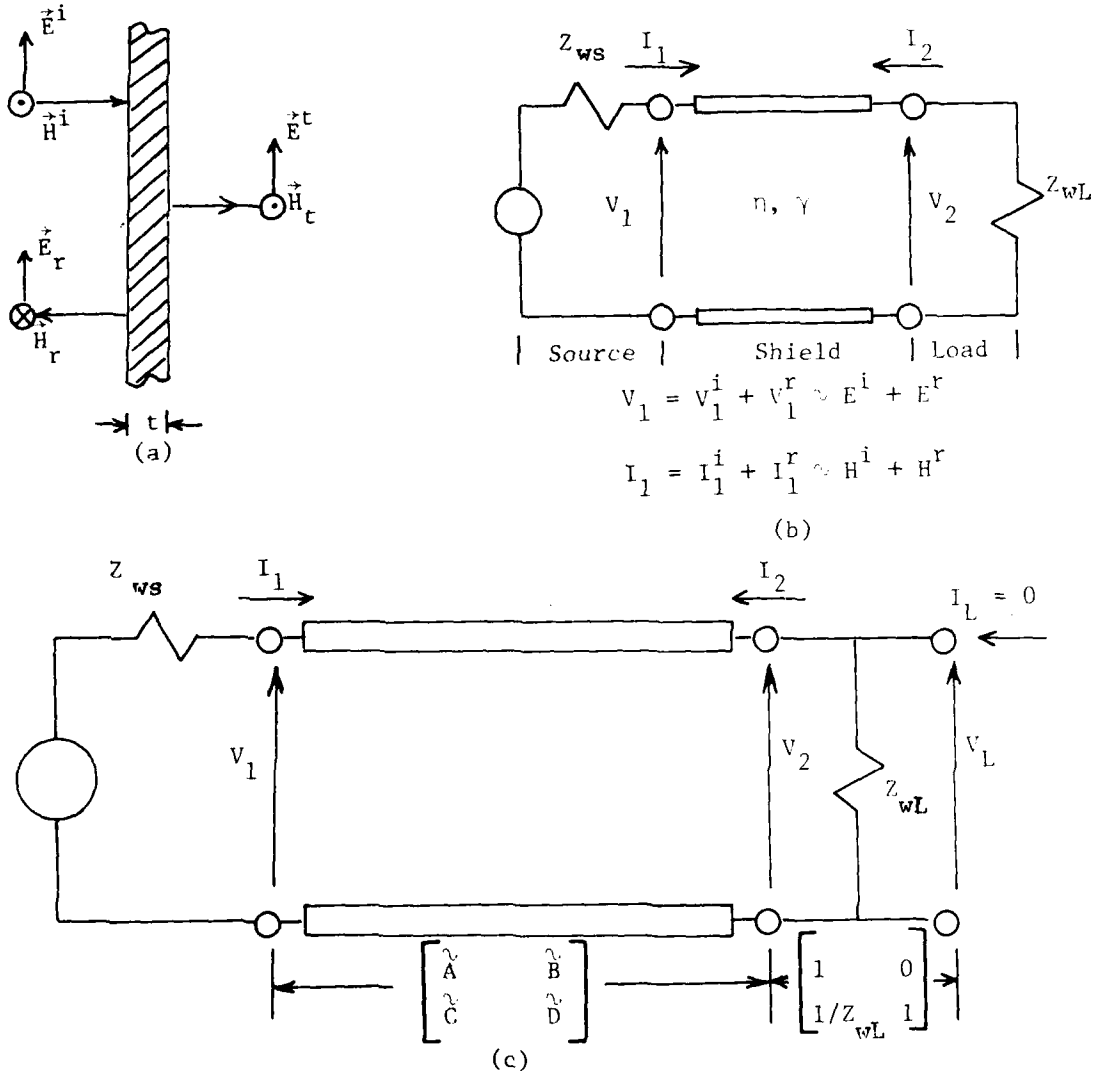

Figure 3. a) Elementary Plane Wave Shielding
b) Transmission Line Analogy
c) ABCD Parameter Representation

$$\rho_{in} = \frac{Z_{in} - Z_{ws}}{Z_{in} + Z_{ws}} = \frac{\frac{V_1}{I_1} - Z_{ws}}{\frac{V_1}{I_1} + Z_{ws}} = \frac{A_T - Z_{ws}\, C_T}{A_T + Z_{ws}\, C_T} = \text{Input Reflection Coefficient}$$

where Z_{in} is the input impedance to the 2-port and other circuit quantities are defined in Figure 3.

Substituting from equations (1) and (3) and (2) and solving for

$\frac{V_1^i}{V_2}$ and $\frac{-I_1^i}{I_2}$ yields:

$$\frac{V_1^i}{V_2} = \frac{1}{2}\left\{\left[1 + \frac{Z_{ws}}{Z_{wL}}\right]\cosh\theta + \left[\frac{\eta}{Z_{wL}} + \frac{Z_{ws}}{\eta}\right]\sinh\theta\right\} \tag{4}$$

= Reciprocal of the electric shielding ratio

$$\frac{-I_1^i}{I_2} = \frac{1}{2}\left\{\left[\frac{Z_{wL}}{Z_{ws}} + 1\right]\cosh\theta + \left[\frac{\eta}{Z_{ws}} + \frac{Z_{wL}}{\eta}\right]\sinh\theta\right\} \tag{5}$$

= Reciprocal of the magnetic shielding ratio.

Then,

$$\text{Magnetic Shielding Effectiveness} = -20 \log_{10}\left|\frac{I_2}{-I_1^i}\right| \text{ and} \tag{6}$$

$$\text{Electric Shielding Effectiveness} = -20 \log_{10}\left|\frac{V_2}{V_1^i}\right|. \tag{7}$$

Notice that magnetic and electric shielding ratios are identical if $Z_{ws} = Z_{wL}$, i.e., for $Z_{wL} = Z_{ws} = Z_o$, the inverse ratios are

$$\frac{V_1^i}{V_2} = \frac{-I_1^i}{I_2} = \cosh\theta + \frac{1}{2}\left(\frac{\eta}{Z_o} + \frac{Z_o}{\eta}\right)\sinh\theta. \tag{8}$$

By proper choice of Z_{wL} and Z_{ws} to match the incident wave characteristics, it is possible to use equations (4), (5), and (8) as very good approximations to a number of other more complex shielding configurations. Physically this is true because the wavelength is typically much smaller within the shield material than outside. In most shield configurations shield thickness is small compared with shield radii of curvature, and to the characteristics of sources utilized in certain measurement structures.

Multilayer shields are easily handled by using the cascading property of ABCD parameters as shown in Figure 4. Having obtained the effective ABCD parameters of the multilayer shield, equations (4), (5), and (8) are used as before to evaluate the various shielding requirements.

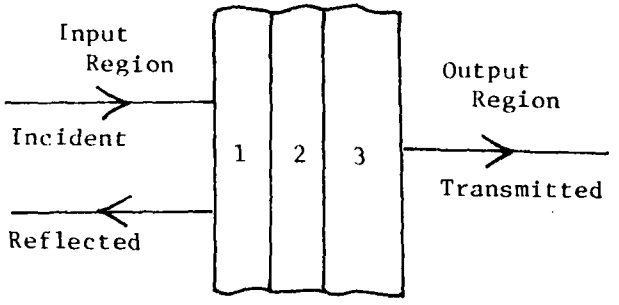

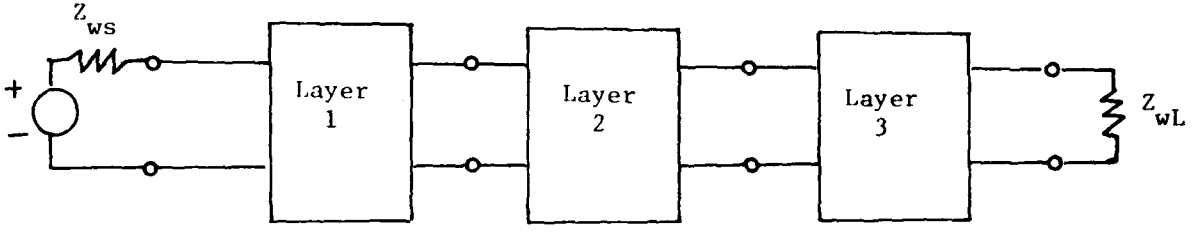

$$\begin{bmatrix} \tilde{A}_T & \tilde{B}_T \\ \tilde{C}_T & \tilde{D}_T \end{bmatrix} = \begin{bmatrix} \tilde{A}_1 & \tilde{B}_1 \\ \tilde{C}_1 & \tilde{D}_1 \end{bmatrix} \begin{bmatrix} \tilde{A}_2 & \tilde{B}_2 \\ \tilde{C}_2 & \tilde{D}_2 \end{bmatrix} \begin{bmatrix} \tilde{A}_3 & \tilde{B}_3 \\ \tilde{C}_3 & \tilde{D}_3 \end{bmatrix}$$

$$\text{Shielding (dB)} = 10 \log_{10} \left| \frac{\tilde{A}_T A_{wL} + \tilde{B}_T + Z_{wL} Z_{ws} \tilde{C}_T + Z_{ws} \tilde{D}_T}{Z_{ws} + Z_{wL}} \right|^2$$

Figure 4. "ABCD" Parameters Simplify Multilayer Shield Analysis

The plane wave shielding given above is used as a "reference" throughout this report. Each new configuration is, where possible, mathematically related to the reference plane-wave configuration. For example, as will be shown, it is possible to relate both transfer impedance and two-loop/flat plate data to the above model.

The transmission-line model of isotropic shields can be extended to handle plane waves incident at oblique angles [5]. The required modification is straight forward, and only the characteristic impedance and propagation factor must be changed.

3.2 Coupling Mechanisms

Four basic coupling mechanisms [6] degrade the performance of a shield. The mechanisms are skin diffusion, aperture coupling, joint coupling and TEM penetration.

Consider a solid (no apertures, seams, etc.) shield. An impinging electromagnetic field establishes a current density on the exterior surface of the shield. That current density penetrates by diffusion to the interior surface of the shield where a tangential electric field is establsiehd. The proportionality factor between the interior tangential electric field and the exterior surface current is called the surface transfer impedance. The overall electromagnetic energy transfer by this mechanism is called skin diffusion. Skin diffusion is controlled by proper choice of material thickness, conductivity and permeability.

Aperture coupling occurs as the result of an external field exciting holes, cracks, windows or other openings in the shield. The field established in the aperture by the external field then couples to the internal region. The effects are typically difficult to calculate exactly for a variety of reasons including strange aperture shapes, complicated and changing interior and exterior environments. Computer programs such as IEMCAP use shape approximations and other idealizations to predict aperture response. Aperture coupling is controlled by proper use of screens, metallic coatings, rf gaskets, etc.

Well formed joints in shield materials (i.e., joints of uniform construction and good electrical contact without large apertures or cracks) may still provide a coupling mechanism via the change in surface impedance experienced in crossing the joint. Such joints usually are described in terms of a distributed joint transfer admittance per unit of joint width.

TEM penetration is the result of induced currents propagating along wires, cables, antenna feeds or other conducting paths into the shielded area. These currents are transmission-line-like currents (hence the name TEM). This mode of coupling can cause further problems by the induced currents generating a field along the wire which may at a distant point induce other troublesome currents in some circuit thought to be well shielded.

3.3 Two-loop/Infinite Flat Plate Configuration

This configuration (Figure 5), with the two loops parallel to the flat plate having a common axis and spaced such that the flat plate lies in the near

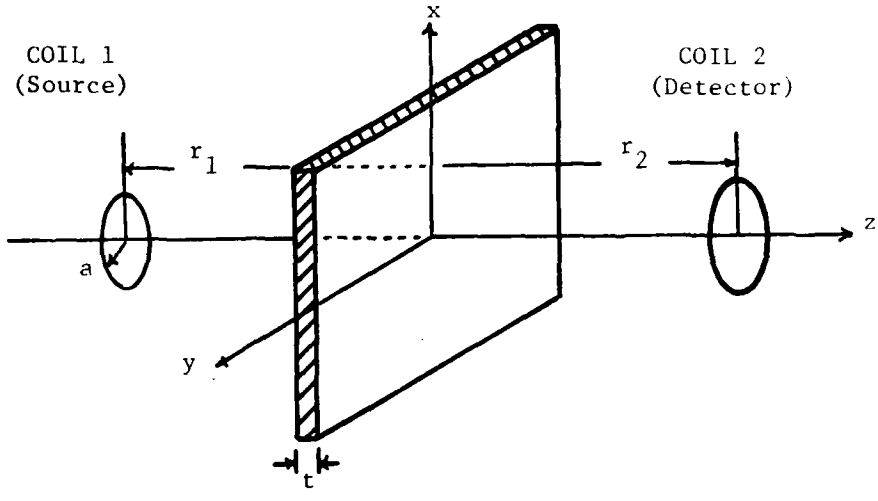

Figure 5. Two-loop/Infinite Flat Plate Configuration

field of the loops, is closely related to several popular and useful configurations for measuring the shielding effectiveness to low-impedance waves. The low-impedance (magnetic field dominates) waves as viewed at the flat plate result from being in the near field of the loops. Note that the wave impedance of the impinging wave varies over the surface of the plate as a function of distance from the source. If the coil-to-plate spacing is a small fraction of a wave length, most of the energy is concentrated within a narrow zone under the coil so that in approximate representations a constant source wave impedance may be used with little error.

Shielding data from configurations of this type for fiber-reinforced laminates have simple interpretations only for materials which are essentially isotropic in the plane of the flat plate, e.g., for multi-layer, mixed orientation graphite laminates but not for unidirectional samples. This restriction is a consequence of the need for roughly circular currents to flow in the plane of the flat plate if the incident magnetic field (which is largely perpendicular to the plate) is to be terminated.

Configurations for which the two-loop/infinite flat plate configuration serves as a useful approximate model include a variety of box-like structures [6] with the flat plate shield forming a partition and undesired leakage between loops inhibited by the enclosure. Such configurations are typically used at frequencies below 100 MHz. Care must be taken, however, since box resonances can obscure the shield's properties.

Moser [7] and Bannister [8, 9] have provided an integral equation solution for the shielding effectiveness of the two-loop/infinite flat plate geometry assuming uniform current in the loops. It is assumed that the shield is a good enough conductor that displacement currents in the shield can be neglected. The complete expression for shielding effectiveness as given by Bannister is given in Appendix A.

As shown in Appendix A, if it is assumed that $r' < \frac{\tau air}{20}$, $\tau_r t > 2$, $\tau_r r' > 10$, $\frac{\tau_r r'}{\mu_r} > 10$, $z \gg t$ and $z \gg a$, where the quantities are defined in the appendix, then

$$S.E._{dB} \simeq 8.686\sqrt{2}\ \tau_r t + 20 \log_{10} \left(\frac{\tau_r z}{8.485\ \mu_r}\right) . \qquad (9)$$

This equation can be shown to be of the same form as the plane wave shielding equation provided an appropriate near-field value is used for the source and load wave impedances. Equation (8) for plane wave shielding can be cast in the well-known Schelkunoff form [2] using the following parameter definitions

$$k = \frac{Z_o}{\eta} \qquad q = \left(\frac{k - 1}{k + 1}\right)^2 \qquad p = \frac{4k}{(k + 1)^2} \qquad (10)$$

Using the above parameters equation (8) can be written as:

$$\text{Inverse Shielding Ratio} = \frac{1}{p}(1 - q\varepsilon^{-2\theta})\varepsilon^{\theta} \quad . \tag{11}$$

Shielding effectiveness is then:

$$S.E._{dB} = 20 \log_{10}\left|\frac{1}{p}(1 - q\varepsilon^{-2\theta})\varepsilon^{\theta}\right| \quad . \tag{12}$$

For the present situation, using $Z_o = j\omega\mu_o r_1$ and recognizing $|k| >> 1$, it follows that $q \simeq 1$ and $\frac{1}{p} \simeq k/4$. Furthermore, for $\tau_r t > 2$, the term $20 \log_{10}|1 - q\varepsilon^{-2\theta}|$ is negligible. Thus, equation (12) becomes

$$S.E._{dB} \simeq 8.686\sqrt{2}\ \tau_r t + 20 \log_{10}\left(\frac{\tau_r r_1}{2.828\mu_r}\right) \tag{13}$$

Following Moser, to compensate for the fact that the near field characteristic wave impedance is actually not constant over the shiled, let $r_1 = z/3$. Then equation (13) becomes identical with the simplified Moser formula of equation (9). This indicates that under a class of important measurement conditions the plane-wave shielding equations with appropriate source and load wave impedances yield excellent results. The transmission line analogy thus applies to the configurations discussed in Sections 1.3.1 and 1.3.2. Frequently a symmetric arrangement with $r_1 = r_2 = z/2$ is utilized in measurements.

3.4 Quasistatic Shielding Formulas for Electrically Thin-Shell Ellipsoids

The boundary value problems for certain ellipsoidal-shell shields geometries as shown in Figure 6 have been solved and the corresponding magnetic shielding effectiveness calculated [9]. Following King, formulas for each of the ellipsoidal and degenerate ellipsoidal shielding formulas can be obtained in the same form as the plane wave shielding equations. These formulas are useful in interpreting measured data from flat-plate and quadrax structures as well as spheres and closed cylinders. Using the notation developed for the plane wave shielding to low-impedance impinging waves can be placed in the form

$$\text{Inverse Magnetic Shielding Ratio} \simeq \cosh\theta + \frac{Z_M}{2\eta}\sinh\theta \quad . \tag{14}$$

A similar relationship can be derived for high wave-impedance impinging signals. The equation is of the same form as the above case but with a different wave impedance for the impinging signal.

$$\text{Inverse Electric Shielding Ratio} \simeq \cosh\theta + \frac{Z_E}{2\eta}\sinh\theta \tag{15}$$

Equation (15) is different from that given by Boeing [6] but reduces to the Boeing form as a special case.

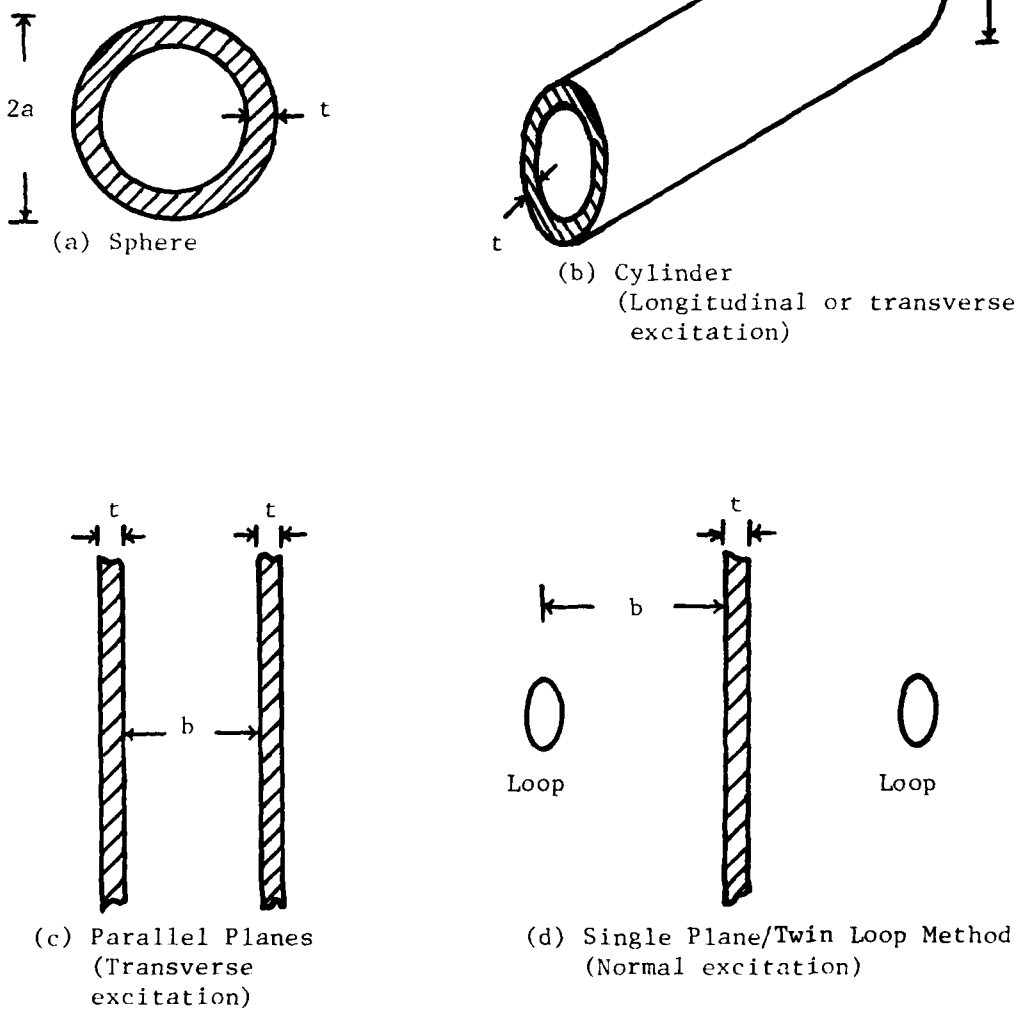

(a) Sphere

(b) Cylinder (Longitudinal or transverse excitation)

(c) Parallel Planes (Transverse excitation)

(d) Single Plane/Twin Loop Method (Normal excitation)

Figure 6. Quasistatic Ellipsoidal Shields.

3.5 Surface Transfer Impedance and Effective Conductivity

Surface transfer impedance has been used for many years as a measure of shielding effectiveness. Combined with other "two-port" parameters it can also be used to characterize shielding materials in computer-aided analysis programs for determining interior and scattered fields of complex geometrical structures [10]. For shields which are thin compared to the radii of curvature of the shield and for which wavelength within the shield is much smaller than that external to the shield, the electromagnetic behavior of the shield is essentially a local phenomena. Each local region may then be considered planar [2]. For a planar shield, the two-port parameters are given in Figure 7.

The impedances Z_{12} and Z_{21} are known as surface transfer impedances since they relate field values at opposite interfaces of the shield. Surface transfer impedance is frequently measured using triaxial or quadraxial configurations [6] and the data are reduced using the Schelkunoff theory [2]. Notice that for electrically thin samples (i.e., small θ) cosh $\theta \simeq 1$ and $Z_{11} \simeq Z_{22} \simeq Z_{12} = Z_{21} = \eta \text{ csch } \theta$. Thus, for electrically thin shields a measurement of the transfer impedance completely describes the shield. For electrically thick samples Z_{11} and Z_{22} are not approximately equal to Z_{12} and additional measurements are required to totally characterize the shield.

From Figure 7 surface transfer impedance written with the new symbol Z_{tr} becomes:

$$Z_{tr} = \eta \text{ csch } \theta \tag{16}$$

Surface transfer impedance can be related to the two-loop/flat-plate configuration through use of the approximations for Equation (9) or the equivalent Equation (14) as follows

$$\begin{matrix}\text{Inverse Magnetic} \\ \text{Shielding Ratio}\end{matrix} = R \simeq \cosh \theta + \frac{Z_M}{2\eta} \sinh \theta \tag{17}$$

Substituting $\frac{\sinh \theta}{\eta} = \frac{1}{\eta \text{ csch } \theta} = \frac{1}{Z_{tr}}$ yields

$$R \simeq \cosh \theta + \frac{Z_M}{2Z_{tr}} . \tag{18}$$

Thus,

$$Z_{tr} \simeq \frac{Z_M}{2(R - \cosh \theta)} \tag{19}$$

For good shields cosh $\theta \simeq 1$ at low frequencies where θ is small (i.e., the shield is electrically thin) and at high frequencies R is much larger than cosh θ. Thus, for reasonably good shields Z_{tr} can be written in terms of the shielding effectiveness measured in the two-loop/flat-plate configuration as

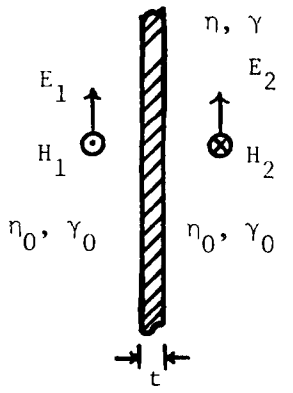

$$E_1 = z_{11}H_1 + z_{12}H_2$$

$$E_2 = z_{21}H_1 + z_{22}H_2$$

where $z_{11} = z_{22} = \eta \coth \theta$

$z_{12} = z_{21} = \eta \operatorname{csch} \theta$

$\theta = \gamma t$

η = wave impedance of shield

γ = propagation factor of shield

Figure 7. Two-port Impedance Representation

Note: $\vec{H}$ and $\vec{E}$ directions assumed cause propagation toward the shield from both left and right side of the shield

$$Z_{tr} \simeq \frac{Z_M}{2(R-1)} \tag{20}$$

where R is obtained from the shielding measurement as

$$R = 10^{\left(\frac{SE_{dB}}{20}\right)}$$

At frequencies where the shield is electrically thin so that θ is sufficiently small that sinh θ can be replaced by θ, it is possible to determine an effective conductivity directly from Z_{tr} in a very simple manner. Such scalar conductivity numbers, as mentioned earlier, seem meaningful for multi-layer, mixed orientation, graphite laminates, but not for unidirectional graphite laminates. Assuming a scalar effective conductivity σ_{eff} in the plane of the laminate and recognizing that for reasonably good conductors

$$\gamma \simeq (1+j)\sqrt{\pi f \mu \sigma_{eff}} = \sigma_{eff}\eta,$$

then

$$Z_{tr} = \frac{\eta}{\sinh\theta} \simeq \frac{(1+j)\frac{\pi f\mu}{\sigma_{eff}}}{\sinh\left[(1+j)t\sqrt{\pi f\mu\sigma_{eff}}\right]} \tag{21}$$

For small θ, sinh $\theta \simeq \theta$, so that

$$Z_{tr} \simeq \frac{(1+j)\frac{\pi f\mu}{\sigma_{eff}}}{t(1+j)\sqrt{\pi f\mu\sigma_{eff}}} = \frac{1}{\sigma_{eff}t}. \tag{22}$$

Thus, for small θ

$$\sigma_{eff} \simeq \frac{1}{tZ_{tr}} \tag{23}$$

For larger θ, σ can be obtained by solving the transcendental equation

$$Z_{tr}\sinh\theta - \eta = 0 \tag{24}$$

The phase of Z_{tr} has not been measured in past experiments, but would clearly be needed if Z_{tr} were to be used to characterize a material in system analysis programs.

The form of the approximation given in Equation (23) is in excellent agreement with measured data given by Boeing [6] with varying thickness. Calculated conductivities seem to be in agreement with results from measurements by other techniques discussed in Sections 2.0 and 3.0.

As an example of the correspondence between two-loop/flat-plate measurements and surface transfer impedance measurements, consider the 24-ply T-300/5208 graphite samples measured by Boeing [6]. The samples were cross-ply layups (0°/45°/90°).

At 1 MHz the measured magnetic shielding from the two-loop/flat-plate configuration is M.S.E. = 16 dB. Thus, $R = 10^{0.8} = 6.31$ and for a loop-to-plate spacing of 1 inch and $|Z_M| = |j\omega\mu_o b| = 0.201$ ohm.

Then

$$|Z_{tr}| \simeq \frac{Z_M}{2(R-1)} = \frac{0.201}{2(5.31)} \simeq 1.9 \times 10^{-2} \text{ ohm}$$

as calculated from the two-loop/flat-plate measurement data. The corresponding 1 MHz direct measured value of surface transfer impedance is

$$|Z_{tr}| \simeq 1.8 \times 10^{-2} \text{ ohm}$$

as measured in the quadrax configuration. The agreement is excellent.

For the same material at 1 MHz

$$\sigma_{eff} \simeq \frac{1}{|Z_{tr}|t} = \frac{1}{(1.8 \times 10^{-2})(24 \times 5.25 \times 10^{-3} \times 2.54 \times 10^{-2})} \simeq 1.73 \times 10^{4} \text{mhos/m}$$

for T-300/5208 Cross-ply layup at 1 MHz.

Similar calculations for 12-ply HTS/5208 graphite show excellent agreement between flat-plate and quadrax data and indicate

$$\sigma_{eff} \simeq 1.5 \times 10^{4} \text{ mhos/m}$$

for HTS/5208 cross-ply layup at 1 MHz.

3.6 Transverse Flat Plate Samples in Waveguide and Transmission Line Structures

Transmission loss and phase measurements on a flat plate sample completely filling the transverse section of a waveguide or transmission line structure can be utilized to characterize a material electromagnetically [11]. Provided the reflections from the sample are not too large, conductivity and permittivity can be determined analytically from the measured insertion loss and phase. Reference [11] provides a complete discussion on limitations of the solution procedure. Typical arrangements for rectangular waveguide and coaxial line structures are shown in Figure 8. The analysis of these and other structures can be carried out simultaneously through the use of the generalized transmission line analogy [2].

3.6.1 General Case

Following Schelkunoff's procedure [2], let each section of the measurement structure be represented by a section of generalized transmission line. The geometry being discussed is shown in Figure 9. The characteristic impedances of the equivalent transmission lines are interpreted as the wave impedance of the actual structure. Equivalent transmission line propagation factors are equal to the corresponding factor of the real structure.

From Figure 8,

$$\begin{bmatrix} V_P \\ I_P \end{bmatrix} = \begin{bmatrix} \tilde{A} & \tilde{B} \\ \tilde{C} & \tilde{D} \end{bmatrix} \begin{bmatrix} V_Q \\ -I_Q \end{bmatrix} \tag{25}$$

where

$$I_Q = -V_{Q/Z_{03}} \qquad \theta = \gamma t$$

$$\tilde{A} = \cosh \theta \qquad \tilde{B} = Z_{02} \sinh \theta$$

$$\tilde{C} = \frac{\sinh \theta}{Z_{02}} \qquad \tilde{D} = \cosh \theta \ .$$

From equation (25), it can be shown that

$$\frac{I_Q}{I_P} = \frac{-Z_{02}}{Z_{02}\cosh \theta + Z_{03}\sinh \theta} \tag{26}$$

$$\frac{V_Q}{V_P} = \frac{Z_{03}}{Z_{03}\cosh \theta + Z_{02}\sinh \theta} \tag{27}$$

Let the total impedance at P looking toward Q be equal to Z_P (note, Z_P includes effects of both interfaces). Then,

$$V_P = \tau_v V_i = \frac{2Z_P}{Z_{01} + Z_P} V_i \tag{28}$$

$$I_P = \tau_I I_i = \frac{2Z_{01}}{Z_{01} + Z_P} I_i \tag{29}$$

where V_i, I_i are the incident voltage and current, respectively, and

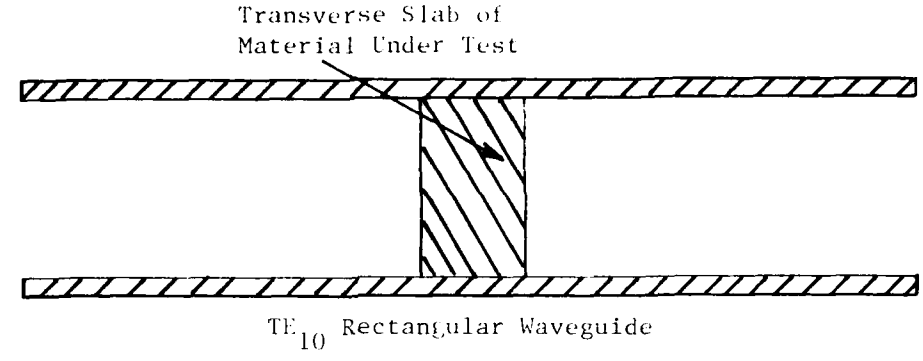

(a)

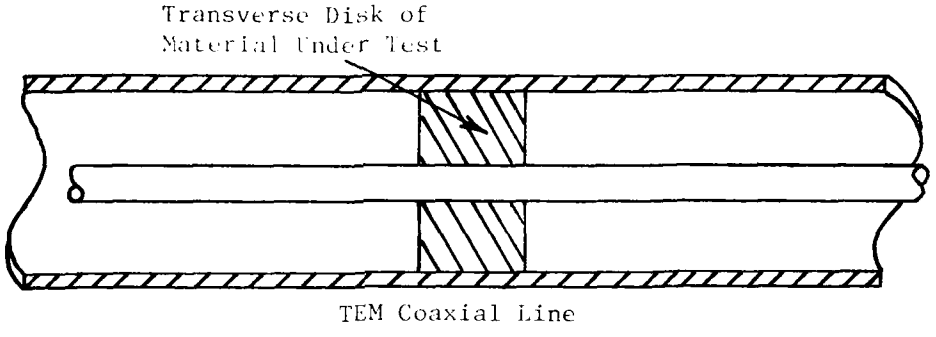

(b)

Figure 8. Two Types of Measurement Strucutres Included in the Generalized Analysis

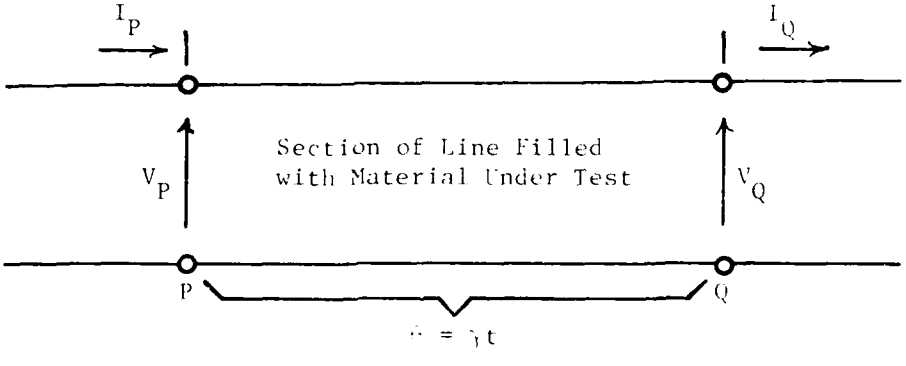

Figure 9. Generalized Transmission Line Model for Measurement Structure. Note: $V_P = V_i + V_r$, $I_P = I_i - I_r$.

$$Z_P = Z_{02}\left[\frac{Z_{03}\cosh\Theta + Z_{02}\sinh\Theta}{Z_{02}\cosh\Theta + Z_{03}\sinh\Theta}\right] = \frac{V_P}{I_P} \quad . \tag{30}$$

Replacing cosh Θ and sinh Θ by their exponential equivalents and substituting from Equations (26) to (30) into Equation (25), the following result is obtained (after considerable algebra).

$$T_I = \frac{-I_Q}{I_i} = \frac{(1 + \rho_{v,P})(1 - \rho_{v,Q})\varepsilon^{-\Theta}}{1 - \rho_{v,P}\rho_{v,Q}\varepsilon^{-2\Theta}} \tag{31}$$

where T_I = overall current transmission coefficient across the section PQ

$\rho_{v,P} = \dfrac{Z_{01} - Z_{02}}{Z_{01} + Z_{02}}$ = interface voltage reflection coefficient at P

$\rho_{v,Q} = \dfrac{Z_{03} - Z_{02}}{Z_{03} + Z_{02}}$ = interface voltage reflection coefficient at Q.

It can be shown that the overall voltage transmission coefficient across the section PQ is

$$T_V = \frac{V_Q}{V_i} = \frac{Z_{03}}{Z_{01}} T_I \quad . \tag{32}$$

If structures 1 and 3 are identical then

$$T = T_I = T_v = \frac{(1 - \rho_v^2)\varepsilon^{-\Theta}}{1 - \rho_v^2\varepsilon^{-2\Theta}} \tag{33}$$

where

$$\rho_v = \frac{Z_{01} - Z_{02}}{Z_{01} + Z_{02}}$$

Insertion loss is thus

$$\text{I.L.} = -20 \log_{10}|T| \tag{34}$$

and the insertion phase is

$$\Delta\phi = \angle T = \text{Angle of Transmission Coefficient}$$

Given measured values of insertion loss and insertion phase for a specified structure, Equation (33) can be solved for the conductivity and the real part of the permittivity of the material under test. This procedure is demonstrated in Section 3.6.2 for a rectangular waveguide measurement system.

3.6.2 Rectangular Waveguide

As a particular case of the preceeding analysis, let the transmission structure be TE_{10} rectangular waveguide with region 2 consisting of a section of guide of width "a," height "b" and length "t," totally filled with the material under test. Further assume that the material can be represented as a lossy dielectric with $\mu = \mu_o$, $\varepsilon = \varepsilon_o \varepsilon_r'$ $(1 - j\tan\delta)$. $\tan\delta$ is the loss tangent of the material and ε_r' is the real part of the permittivity. Regions 1 and 3 are air-filled and have the same width and height as section 2.

$$Z_{TE}^1 = \frac{\eta_o}{\sqrt{1-\left(\frac{\lambda_o}{\lambda_c}\right)^2}} = \text{Wave impedance of regions 1 and 3} \tag{36}$$

$$Z_{TE}^2 = \frac{\eta_2}{\sqrt{1-\left(\frac{\lambda_2}{\lambda_c}\right)^2}} = \frac{1}{\sqrt{\varepsilon_r}} \frac{\eta_o}{\sqrt{1-\left(\frac{\lambda_o}{\sqrt{\varepsilon_r}\lambda_c}\right)^2}} = \text{Wave impedance of region 2} \tag{37}$$

where $\eta_o = \sqrt{\frac{\mu_o}{\varepsilon_o}}$ $\quad \eta_2 = \sqrt{\frac{\mu_o}{\varepsilon_2}}$

$\varepsilon_r = \varepsilon_r' (1 - j\tan\delta)$, $\quad \lambda_2 = \frac{\lambda_o}{\sqrt{\varepsilon_r}}$

λ_o = wavelength in freespace at measurement frequency

λ_c = cutoff wavelength (e.g. 2a in air-filled waveguide)

Also,

$$\rho_v = \frac{Z_{TE}^1 - Z_{TE}^2}{Z_{TE}^1 + Z_{TE}^2} \tag{38}$$

$$\theta = \gamma t = j\omega\sqrt{\mu_o \varepsilon_o}\sqrt{\varepsilon_r - \left(\frac{\lambda_o}{\lambda_c}\right)^2}\, t. \tag{39}$$

Substitution into Equation (33) yields the desired result.

Given measured values of insertion loss and phase, Equation (33) can now be solved for ε_r' and tan δ. The conductivity, σ. is related to the loss tangent, tan δ^r, by $\sigma = \omega\varepsilon_r'\varepsilon_o$ tan δ. An iterative numerical procedure [12] is used to solve Equation (33). For relatively high conductivity, materials such as graphite epoxy, insertion loss and phase are quite insensitive to variations in ε_r', as shown in Figure 10. It is then exceptionally difficult to determine accurate values of ε_r' from measured insertion loss and phase by solving Equation (33). If ε_r' is independently known, accurate conductivity values can be obtained.

4.0 Scattering Parameter Techniques

The ease with which scattering parameters can be measured [4, 13] makes them especially well suited for describing distributed circuits and most electromagnetic propagation problems. The simple direct relationship between scattering parameters and transmitted and reflected power is an added advantage in interpreting results.

4.1 Definitions

Generalized scattering parameters have been defined by K. Kurokawa [2, 14]. These parameters describe the interrelationships of a new set of variables (a_i, b_i). The variables a_i and b_i are normalized complex voltage waves incident on and reflected from the ith port of the system. They are defined in terms of the terminal voltage V_i, and an arbitrary reference impedance Z_i, as follows:

$$a_i = \frac{V_i + Z_i I_i}{2\sqrt{|R_e Z_i|}} \tag{40}$$

$$b_i = \frac{V_i - Z_i^* I_i}{2\sqrt{|R_e Z_i|}} \tag{41}$$

where the asterisk denotes complex conjugate.

For most measurements and calculations it is convenient to assume that the reference impedance Z_i is positive and real. For the remainder of this report, all variables and parameters in scattering analysis will be referenced to a single real impedance R_0. Other normalization schemes are useful in some cases. Generalized normalization is discussed in the literature [2, 14].

The quantities used in defining S-parameters for a 2-port system are shown in Figure 11. The independent variables a_1 and a_2 are normalized incident voltages (or the corresponding analog quanitity), as follows:

$$a_1 = \frac{V_1 + I_1 R_0}{2\sqrt{R_0}} = \frac{\text{voltage wave incident on port 1}}{\sqrt{R_0}} = V_{i1}/\sqrt{R_0} \tag{42}$$

(42)

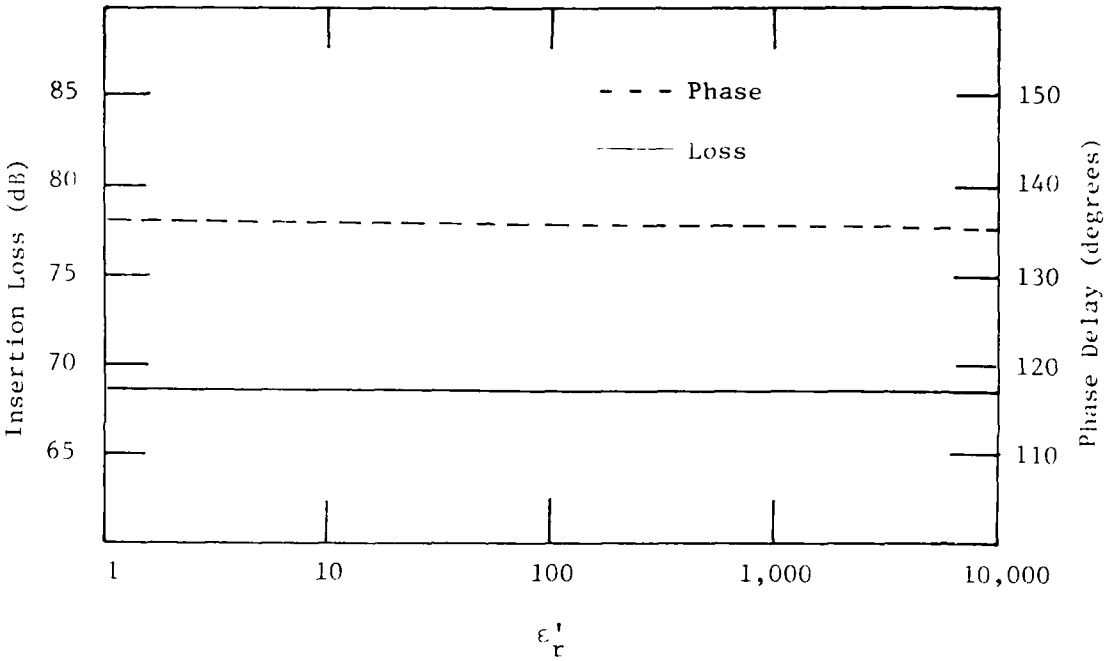

Figure 10. Insertion loss and phase delay for a lossy transverse slab in L-band rectangular waveguide, t = 0.02 inches, $\sigma = 10^4$ mhos/m. Loss and phase are both essentially independent of ε_r'.

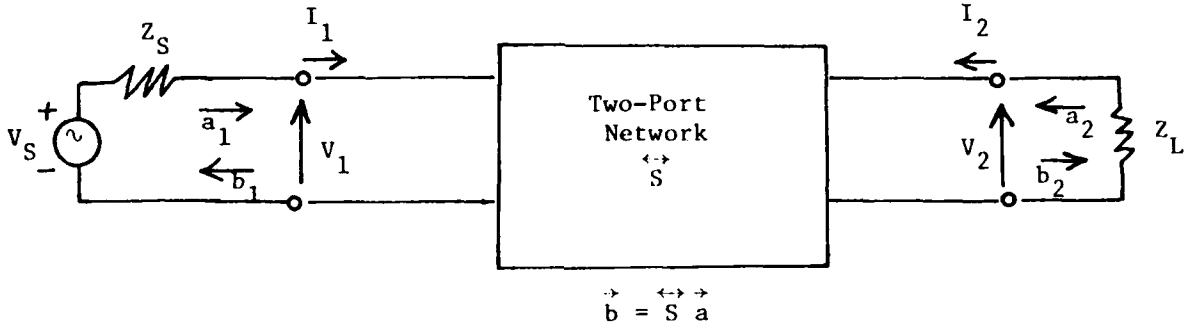

Figure 11. Two-port network showing incident (a_1, a_2) and reflected traveling waves (b_1, b_2) used in S-parameter definitions.

$$a_2 = \frac{V_2 + I_2 R_0}{2\sqrt{R_0}} = \frac{\text{voltage wave incident on port 2}}{\sqrt{R_0}}$$

$$= \frac{V_{i2}}{\sqrt{R_0}} \tag{43}$$

Dependent variables b_1 and b_2 are normalized reflected voltages:

$$b_1 = \frac{V_1 - I_1 R_0}{2\sqrt{R_0}} = \frac{\text{Voltage wave reflected (or emanating) from port 1}}{\sqrt{R_0}} = \frac{V_{r1}}{\sqrt{R_0}} \tag{44}$$

$$b_2 = \frac{V_2 - I_2 R_0}{2\sqrt{R_0}} = \frac{\text{Voltage wave reflected (or emanating) from port 2}}{\sqrt{R_0}} = \frac{V_{r2}}{\sqrt{R_0}} \tag{45}$$

The linear equations describing the 2-port are of the form:

$$\vec{b} = \overleftrightarrow{S}\,\vec{a} \quad \text{or}$$

$$b_1 = S_{11}a_1 + S_{12}a_2 \tag{46}$$

$$b_2 = S_{21}a_1 + S_{22}a_2 \tag{47}$$

The S-parameters S_{11}, S_{12}, S_{21} S_{22} are:

$$S_{11} = \left.\frac{b_1}{a_1}\right|_{a_2=0} = \text{Input reflection coefficient with the output port terminated by a "matched" load } (Z_L = R_0 \text{ sets } a_2 = 0). \tag{48}$$

$$S_{22} = \left.\frac{b_2}{a_2}\right|_{a_1=0} = \text{Output reflection coefficient with the input port terminated by a "matched" load } (Z_S = R_0 \text{ and } V_S = 0). \tag{49}$$

$$S_{21} = \left.\frac{b_2}{a_1}\right|_{a_2=0} = \text{Forward transmission (insertion) gain (or loss) with the output port terminated in a "matched" load.} \tag{50}$$

$$S_{12} = \left.\frac{b_1}{a_2}\right|_{a_1=0} = \text{Reverse transmission (insertion) gain (or loss) with the input port terminated in a "matched" load.} \tag{51}$$

The relationships between a_1, a_2, b_1, b_2 and the various power waves of interest are given by

$|a_1|^2$ = Power incident on the input port

= Power available from a source of impedance R_0

$|a_2|^2$ = Power incident on the output port

= Power reflected from the load

$|b_1|^2$ = Power reflected from the input port

= Power available from a R_0 source minus the power delivered to the input port

$|b_2|^2$ = Power reflected or emanating from the output port

= Power incident on the load

= Power that would be delivered to a R_0 load

Hence S-parameters are directly related to power gain and mismatch loss, quantities which are often of more interest than the corresponding voltage functions:

$$|S_{11}|^2 = \frac{\text{Power reflected from the input port}}{\text{Power incident on the input port}}$$

$$|S_{22}|^2 = \frac{\text{Power reflected from the output port}}{\text{Power incident on the output port}}$$

$$|S_{21}|^2 = \frac{\text{Power delivered to a } R_0 \text{ load}}{\text{Power available from a } R_0 \text{ load}}$$

= Transduce power gain with R_0 load and source

$|S_{12}|^2$ = Reverse transducer power gain with R_0 load and source.

4.2 System Calculations with Scattering Parameters

Scattering parameters are particularly convenient in calculating transmitted and reflected power or related quantities such as shielding effectiveness. The transfer parameters S_{12} and S_{21} are a measure of the complex insertion gain, and the driving-point parameters S_{11} and S_{22} are a measure of the input and output mismatch (i.e., reflection) loss. As dimensionless expressions of gain and reflection, the parameters not only give a clear and meaningful physical interpretation of the system performance but also form a natural set of parameters for use with signal flow graphs [15]. It is not necessary to use signal flow graphs in order to use S-parameters, but flow graphs greatly simplify S-parameter calculations.

In a signal flow graph each port is represented by two nodes (one for each variable). Node a_n represents the wave coming into the system at port n and node b_n represents the wave leaving the system at port n. The complex scattering coefficients are then represented as multipliers on branches connecting the nodes within the system and in adjacent systems. Figure 12 summarizes the above statements and presents the flow graph representation of the 2-port system shown in Figure 11.

The simplification of system analysis by signal flow graphs results from the application of the "non-touching loop rule" as described in [15] and summarized in Figure 13. A first order loop is defined as the product of the branches encountered in moving from a node in the direction of the arrows back to that original node. A second order loop is defined as the product of any two non-touching first order loops. Nontouching loops have no nodes in common. An n^{th} order loop is defined as the product of any n non-touching first order loops. This rule applies the generalized formula of Figure 13 to determine the transfer function between any two nodes within a system. The non-touching loop rule is applied to calculating the transducer power gain of a 2-port system in Figure 14.

Cascading of 2-port systems is easily accomplished through use of signal flow graphs and the S-parameter definitions given in Equations (46-51). The cascading is easiest if done 2 systems at a time. This process and the resulting combined S-parameters are illustrated in Figure 15.

4.3 Parameter Relationships for Two-Ports

It is convenient at times to be able to convert between the various parameter representations for 2-port networks. The equations below provide those conversion relations most useful in shielding analysis. Other conversions are in the literature [3, 4].

4.3.1 Z to S

Given a normalized impedance matrix

$$\overleftrightarrow{Z} = \begin{bmatrix} Z_{11} & Z_{12} \\ Z_{21} & Z_{22} \end{bmatrix} \tag{52}$$

the corresponding S-matrix is

$$\overleftrightarrow{S} = \begin{bmatrix} S_{11} & S_{12} \\ S_{21} & S_{22} \end{bmatrix} \tag{53}$$

where

- EACH VARIABLE BECOMES A NODE.
- EACH PARAMETER BECOMES A BRANCH.
- BRANCHES ENTER DEPENDENT VARIABLE NODES AND EMANATE FROM INDEPENDENT VARIABLE NODES.
- EACH NODE IS EQUAL TO THE SUM OF THE BRANCHES ENTERING THAT NODE.

$b_1 = S_{11}\, a_1 + S_{12}\, a_2$

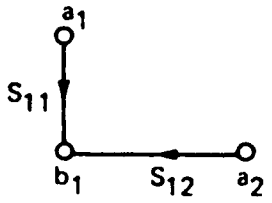

$b_2 = S_{21}\, a_1 + S_{22}\, a_2$

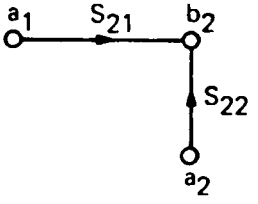

Figure 12. Flow Graph Notation

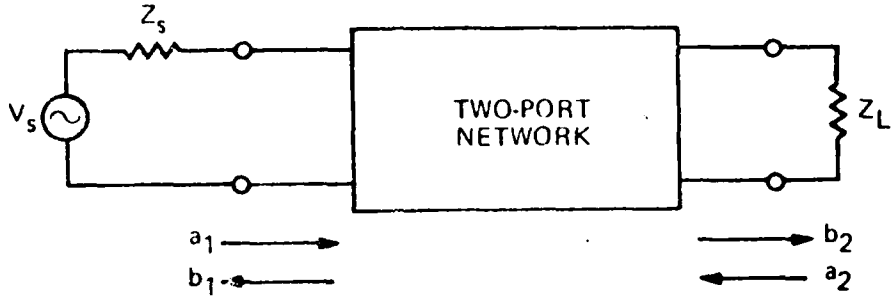

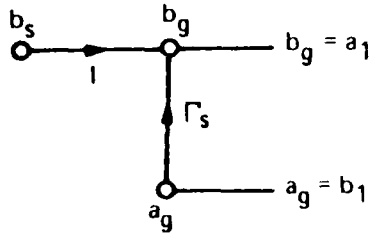

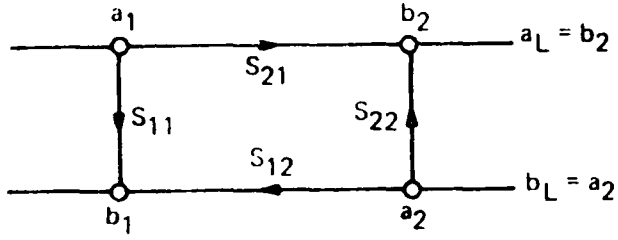

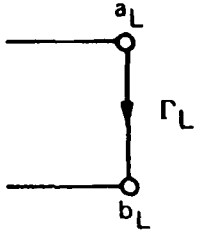

COMPLETE FLOW GRAPH FOR 2-PORT

$$b_s = \frac{V_s\sqrt{Z_o}}{Z_s + Z_o}$$

$$\Gamma_s = \frac{Z_s - Z_o}{Z_s + Z_o}$$

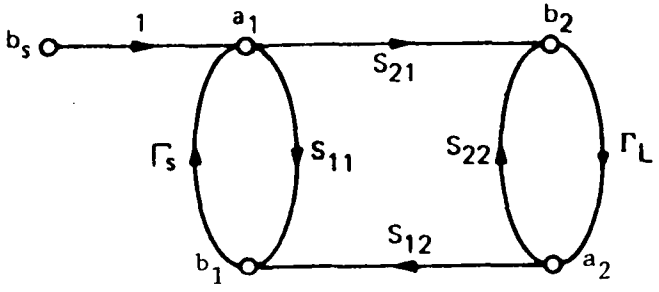

$$\Gamma_L = \frac{Z_L - Z_o}{Z_L + Z_o}$$

Figure 12. (Cont'd)

NONTOUCHING LOOP RULE

$$T = \frac{P_1 \left[1 - \Sigma L(1)^{(1)} + \Sigma L(2)^{(1)} - \Sigma L(3)^{(1)} + \cdots\right] + P_2 \left[1 - \Sigma L(1)^{(2)} + \cdots\right.}{1 - \Sigma L(1) + \Sigma L(2) - \Sigma L(3) + \cdots}$$

WHERE

$\Sigma L(1)$	SUM OF ALL FIRST ORDER LOOPS.
$\Sigma L(n)$	SUM OF ALL nth ORDER LOOPS.
P_1; P_2; etc.	PATHS CONNECTING VARIABLES IN QUESTION.
$\Sigma L(1)^{(1)}$	SUM OF THOSE FIRST ORDER LOOPS WHICH DO NOT TOUCH P_1.
$\Sigma L(n)^{m}$	SUM OF THOSE nth ORDER LOOPS WHICH DO NOT TOUCH P_m.
T	RATIO OF DEPENDENT TO INDEPENDENT VARIABLE.

INPUT IMPEDANCE OF A TWO-PORT WITH ARBITRARY LOAD

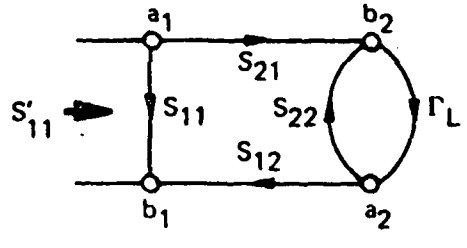

$$P_1 = S_{11} \qquad P_2 = S_{21}\,\Gamma_L\,S_{12}$$

$$L(1) = S_{22}\,\Gamma_L$$

$$S'_{11} = \frac{b_1}{a_1} = \frac{S_{11}(1 - S_{22}\Gamma_L) + S_{21}\Gamma_L S_{12}}{1 - S_{22}\Gamma_L}$$

$$\boxed{S'_{11} = S_{11} + \frac{S_{21} S_{12} \Gamma_L}{1 - S_{22}\Gamma_L}}$$

Figure 13. Nontouching Loop Rule for Use in Evaluating Transfer Functions

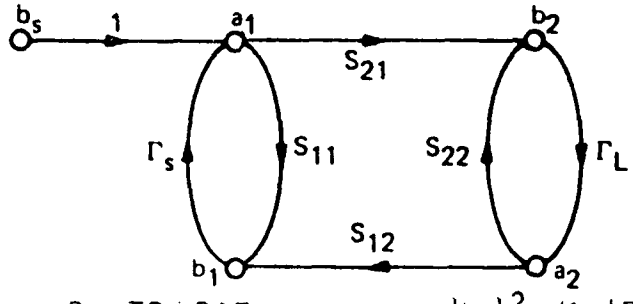

$$G_T = \frac{P_{del\ TO\ LOAD}}{P_{avail\ FROM\ SOURCE}} = \frac{|b_2|^2 \ (1-|\Gamma_L|^2)}{\frac{|b_s|^2}{(1-|\Gamma_s|^2)}}$$

$$\frac{b_2}{b_s} = \frac{S_{21}}{1-S_{11}\Gamma_s - S_{22}\Gamma_L - S_{21}S_{12}\Gamma_L\Gamma_s + S_{11}\Gamma_s S_{22}\Gamma_L}$$

$$G_T = \frac{|S_{21}|^2 \ (1-|\Gamma_s|^2)\ (1-|\Gamma_L|^2)}{|(1-S_{11}\Gamma_s)\ (1-S_{22}\Gamma_L) - S_{21}S_{12}\Gamma_L\Gamma_s|^2}$$

Figure 14. Transduce Power Gain Calculations

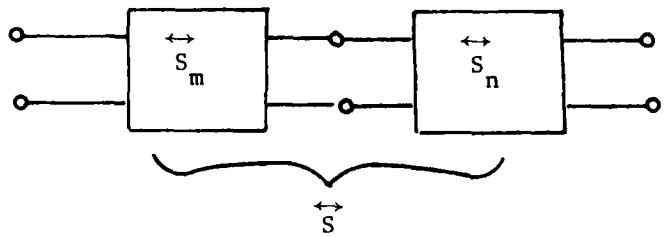

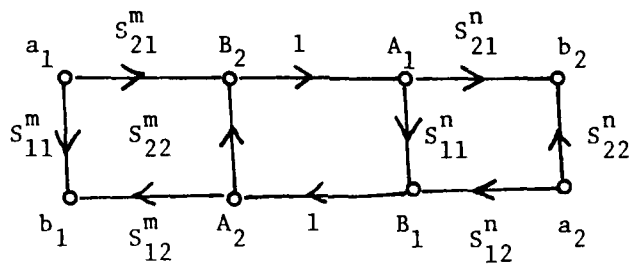

Signal Flow Graph

$$S_{11} = S^m_{11} + \frac{S^m_{12}S^m_{21}S^n_{11}}{1 = S^m_{22}S^n_{11}}$$

$$S_{12} = \frac{S^m_{12}S^n_{12}}{1 - S^m_{22}S^n_{11}}$$

$$S_{21} = \frac{S^m_{21}S^n_{21}}{1 - S^m_{22}S^n_{11}}$$

$$S_{22} = S^n_{22} + \frac{S^n_{12}S^n_{21}S^m_{22}}{1 - S^m_{22}S^n_{11}}$$

Figure 15. Cascading "S" for Multilayer Shield

$$S_{11} = \frac{\Delta_Z + Z_{11} - (Z_{22} + 1)}{\Delta_Z + Z_{11} + Z_{22} + 1}$$

$$S_{12} = \frac{2Z_{12}}{\Delta_Z + Z_{11} + Z_{22} + 1}$$

$$S_{21} = \frac{2Z_{21}}{\Delta_Z + Z_{11} + Z_{22} + 1}$$

$$S_{22} = \frac{\Delta_Z + Z_{22} - (Z_{11} + 1)}{\Delta_Z + Z_{11} + Z_{22} + 1}$$

$$\Delta_Z = Z_{11}Z_{22} - Z_{12}Z_{21} .$$

4.3.2 ABCD to S

Given a normalized ABCD matrix

$$\overleftrightarrow{ABCD} = \begin{bmatrix} A & B \\ C & D \end{bmatrix} \tag{54}$$

the corresponding S-matrix is

$$\overleftrightarrow{S} = \begin{bmatrix} S_{11} & S_{12} \\ S_{21} & S_{22} \end{bmatrix} \tag{55}$$

where

$$S_{11} = \frac{A + B - C - D}{A + B + C + D}$$

$$S_{12} = \frac{2\Delta_{CH}}{A + B + C + D}$$

$$S_{21} = \frac{2}{A + B + C + D}$$

$$S_{22} = \frac{-A + B - C + D}{A + B + C + D}$$

$$\Delta_{CH} = AD - BC .$$

4.4 Multiport Systems

Scattering parameter analysis is easily extended to multiport systems. For a 4-port system the scattering equations would be:

$$\begin{bmatrix} b_1 \\ b_2 \\ b_3 \\ b_4 \end{bmatrix} = \begin{bmatrix} S_{11} & S_{12} & S_{13} & S_{14} \\ S_{21} & S_{22} & S_{23} & S_{24} \\ S_{31} & S_{32} & S_{33} & S_{34} \\ S_{41} & S_{42} & S_{43} & S_{44} \end{bmatrix} \begin{bmatrix} a_1 \\ a_2 \\ a_3 \\ a_4 \end{bmatrix} \tag{56}$$

where

$$S_{11} = \left.\frac{b_1}{a_1}\right|_{a_2=a_3=a_4=0} = \text{Input reflection coefficient at port 1 with matched load at all other ports.}$$

$$S_{21} = \left.\frac{b_2}{a_1}\right|_{a_2=a_3=a_4=0} = \text{Forward transmission (insertion) gain (or loss) with ports 2, 3, 4 all terminated in matched loads.}$$

etc.

The extension to n-ports is straightforward. Multiport techniques are necessary in treating shielding effectiveness of anisotropic shields.

5.0 An Anisotropic Model for Plane Wave Propagation (with Applications to Single and Multilayer Advanced Composites)

Advanced composite materials are laminates made up of a number of individual layers bonded together. Each layer consists of a unidirectional array of long fibers embedded in, and firmly bonded to a matrix. The basic building blocks of any specific composite are the types of fibers and matrix involved. Some fiber/matrix systems are: boron/epoxy, graphite/epoxy, Kevlar/epoxy, graphite/polyimide and graphite/thermoplastic. Other materials contain grids of various conductive wires.

The purpose of this section is to describe a macroscopic electromagnetic model for plane wave propagation through fiber-reinforced and related materials. It is convenient to distinguish between "ply" and "layer." A ply is the basic composite material unit. A layer is made up of plies with uniform fiber orientation. Thus, both plies and layers are unidirectional but a layer may consist of more than one ply. In a multilayer structure, fibers in adjacent layers have different orientations. A multilayer flat panel with arbitrarily polarized incident plane waves is considered. The fibers in each layer may be

oriented in any desired direction permitting both unidirectional and mixed-orientation samples to be considered.

On a microscopic basis advanced composites are clearly both inhomogeneous and anisotropic. From a macroscopic point of view, the fiber spacings are sufficiently close that over a wide frequency range (perhaps dc - 18 GHz) it appears that the inhomogeneities can be averaged out, at least to first order. The anisotropic nature, however, of a unidirectional sample must be taken into account. For mixed orientation, multilayer samples the anisotropic effects are important unless the layers are so thin electrically that considerable layer-to-layer averaging occurs.

Based on the above discussion, it appears reasonable to model each layer as a "quasi-homogeneous" anisotropic material. Both fiber and matrix materials currently under consideration are nonmagnetic so that the permeability of these composite materials can be taken to be essentially μ_o. Both permittivity and conductivity parameters may be anisotropic. It is assumed that the principal axes of the permittivity and conductivity properties are the same so that both the permittivity and conductivity tensors may be diagonalized simultaneously. As a labor saving device the usual combination of conductivity and permittivity into a single complex permittivity tensor is assumed. Two sets of coordinates are utilized as shown in Figure 16. The x, y, z coordinates are the "propagation coordinates," and all the final equations are expressed in terms of xyz-components. The ζ_1 ζ_2, ζ_3 coordinates are called "material coordinates." The material coordinate axes are aligned with the principal directions of the composite material.

Analytically it is possible that the "material axes" ζ_1, ζ_2, ζ_3 within each layer be skewed with respect to each of the "propagation coordinate" axes x, y, z. Physically, however, a laminate is made up of parallel layers with the fibers of adjacent layers lying in parallel planes but having different fiber orientation within the plane, i.e., the material coordinate ζ_3 will usually coincide with z in every layer of a multilayer sample, while the direction of ζ_1, ζ_2 with respect to x, y varies from layer to layer.

5.1 Unidirectional Samples

Consider a unidirectional flat plate of advanced composite material. The principal directions (along the fibers, perpendicular to the fibers but parallel to the plane of the layer, and perpendicular to both the fiber direction and the plane of the layer) are used to define "material" coordinates. Let ζ_1 be parallel to the fibers, ζ_2 perpendicular to the fibers but parallel to the plane, ζ_3 perpendicular to both fibers and the plane of the layer. In these coordinates the complex permittivity matrix is diagonal with each of the three components, in general, different.

$$\overleftrightarrow{\varepsilon} = \begin{array}{c|ccc} & \zeta_1 & \zeta_2 & \zeta_3 \\ \hline \zeta_1 & \hat{\varepsilon}_{11} & 0 & 0 \\ \zeta_2 & 0 & \hat{\varepsilon}_{22} & 0 \\ \zeta_3 & 0 & 0 & \hat{\varepsilon}_{33} \end{array} \qquad (57)$$

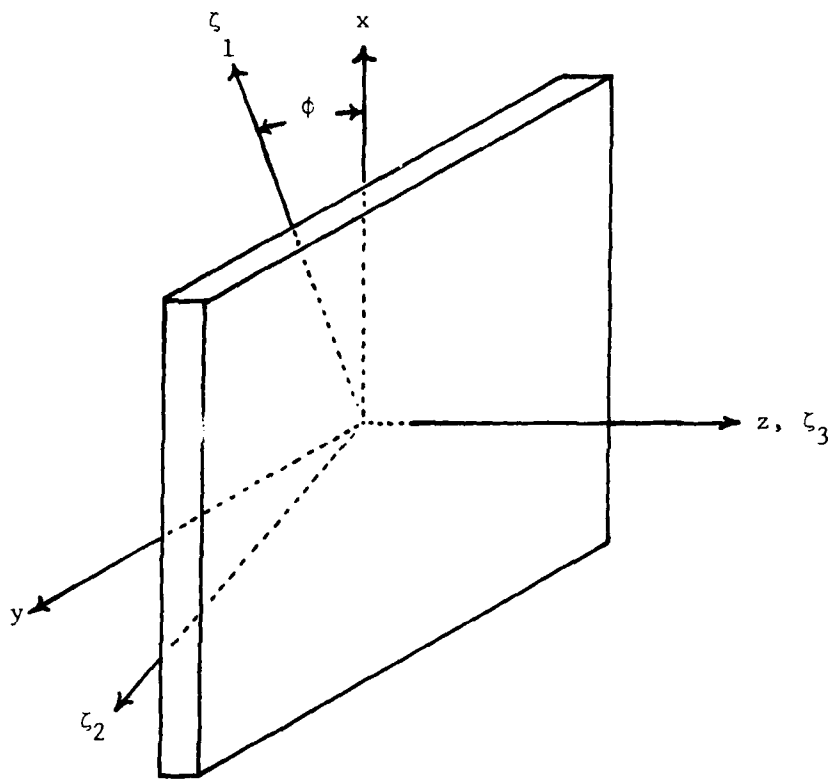

Figure 16. Propagation (x, y, z) and Material (ζ_1, ζ_2, ζ_3) Coordinates for Treating Anisotropic Material with "OpticAxis" in z Direction.

where $\hat{\varepsilon}_{ii} = \varepsilon_{ii} - j\frac{\sigma_{ii}}{\omega}$.

In terms of ζ_1, ζ_2, ζ_3 the complex permittivity tensor $\overleftrightarrow{\hat{\varepsilon}}$ is diagonal. The individual elements of $\overleftrightarrow{\hat{\varepsilon}}$, namely $\hat{\varepsilon}_{ii} = \varepsilon_{ii} - j\frac{\sigma_{ii}}{\omega}$, can be measured or calculated for a single unidirectional sample of each fiber/matrix combination. The matrix in each case is normally a good dielectric while the fibers vary from modest conductors (graphite) to poor dielectrics (boron) to good dielectrics (Kevlar). Thus, the relative importance of ε_{ii} and σ_{ii} in the complex permittivity $\hat{\varepsilon}_{ii}$ is a function of the fiber/matrix combination and frequency.

5.2 Wire Grid Model

Prior to detailed analysis of the rather complicated anisotropic model for fiber-reinforced materials, it is instructive to examine some less complicated geometries [16] to perhaps determine some of the dominant features of shielding to be expected from such materials. Consider an array of infinitely long, identical, parallel, perfectly conducting wires as shown in Figure 17. This is, admittedly, a very crude model, but it is useful in illustrating an important point. Let the wires have a diameter D, and a spacing, S, and let a plane wave having wavelength, λ, be incident normally on the grid. The incident electric field may be polarized either parallel (i.e., $E_{\parallel}$) or perpendicular (i.e., $E_{\perp}$) to the axis of the wires. The equivalent circuit of the grid as seen by the incident wave is given by Marcavitz [17] and is shown in Figure 18. When $S/\lambda << 1$ the circuit parameters are:

$$\frac{X_a}{Z_0} = \frac{S}{\lambda}\left[\ell n\left(\frac{S}{\pi D}\right) + 0.601\left(\frac{S}{\lambda}\right)^2\right] \tag{58}$$

$$\frac{X_b}{Z_0} = \frac{S}{\lambda}\left(\frac{\pi D}{S}\right)^2 \tag{59}$$

$$\frac{B_a}{Y_0} = \frac{S}{2\lambda}\left(\frac{\pi D}{S}\right)^2 \frac{1}{A_2} \tag{60}$$

$$\frac{B_b}{Y_0} = \frac{2\lambda}{S}\left(\frac{S}{\pi D}\right)^2 A_1 - \left(\frac{S}{4\lambda}\right)\left(\frac{\pi D}{S}\right)^2 \frac{1}{A_2} \tag{61}$$

where

$$A_1 = 1 + \frac{1}{2}\left(\frac{\pi D}{\lambda}\right)^2\left(\ell n\,\frac{S}{\pi D} + \frac{3}{4}\right)$$

$$A_2 = 1 + \frac{1}{2}\left(\frac{\pi D}{\lambda}\right)^2\left[\frac{11}{4} - \ell n\,\frac{S}{\pi D}\right] + \frac{1}{24\pi}\left(\frac{\pi D}{S}\right)^2$$

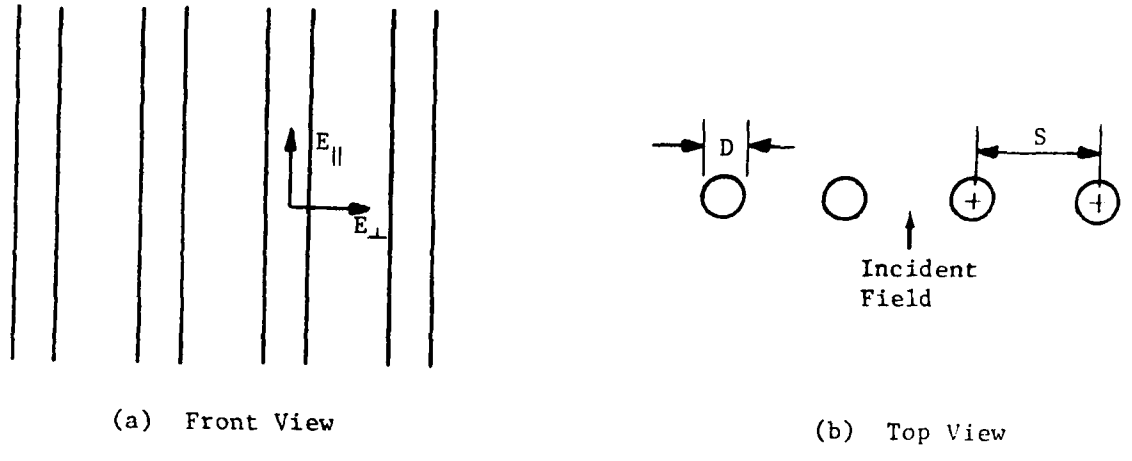

(a) Front View

(b) Top View

Figure 17. Wire Grid Approximation of a Unidirectional Fiber-Reinforced Material (After Bodnar [16])

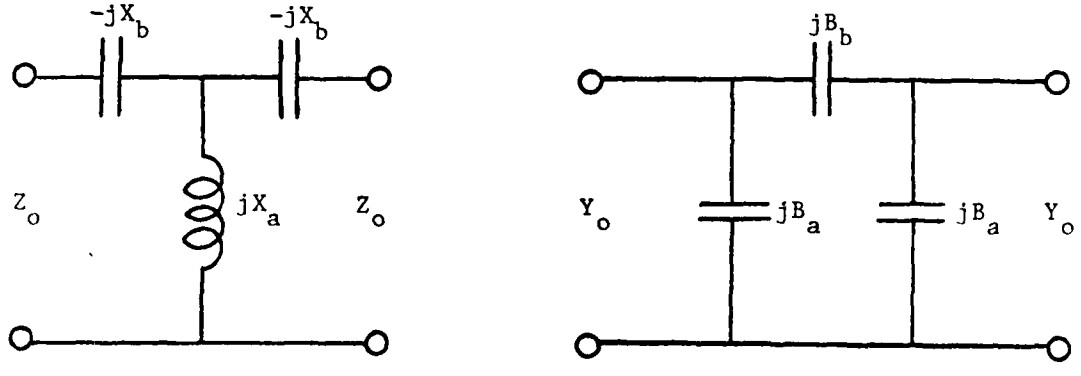

(a) For Parallel Polarization

(b) For Perpendicular Polarization

Figure 18. Equivalent Circuit of Wire Grid at Normal Incidence. (After Bodnar [16])

and Z_0 and Y_0 are the characteristic impedance and admittance of free space, respectively.

Inspection of (58) and (59) shows that X_a and X_b approach zero as λ becomes large, indicating that the inductor of Figure 18a shorts the transmission line at low frequencies and little power is transferred through the wire grid. Thus, the grid acts as an effective shield to parallel polarization at low frequencies. Inspection of (60) and (61) shows that B_a approaches zero and that B_b becomes large as λ becomes large. This indicates that the shunt capacitors in Figure 18b act as open circuits and the series capacitor acts as a short as λ becomes large. This corresponds to a large amount of energy being transferred through the grid and shows that the grid is not a good shield for perpendicular polarization.

How long do the wires have to be in order to obtain good shielding characteristics for parallel polarization? What would the shielding characteristics be if the infinitely long wires of Figure 17 were replaced by a two dimensional array of short nontouching wires? The shielding characteristics now turn out to be bad for both polarizations as will be illustrated below. The conclusion clearly is that a large number of noncontacting fibers will not provide good shielding. Long conducting paths (compared to wavelength??) are necessary for good shielding.

A model for fibers consisting of short, noncontacting plates is shown in Figure 19. Analysis of such structures has been carried out by Chen [18] and Montgomery [19]. General equations are provided by both Chen and Montgomery, but the equations must be programmed for a digital computer to obtain numerical results. Sample calculations are presented by both authors, but no general design information is given. The general trends indicate low attenuation for both polarizations when the plate dimensions are small compared to wavelength. A reasonable conclusion appears to be that noncontacting fibers that are electrically small (i.e., much smaller than a wavelength in their major dimension) do not provide effective shielding at RF frequencies.

5.3 Unidirectional Sample with Normally Incident, Arbitrarily Polarized Plane Wave

Assume an infinite plane sheet of unidirectional material of thickness t oriented perpendicular to the z-direction. Fibers are oriented in the ζ_1-direction as shown in Figure 16. The ζ_3 and z axes are aligned. The direction of propagation of the incident plane wave is +z. The permeability μ is essentially equal to μ_o. Permittivity and conductivity are combined in the complex permittivity tensor given by equations (57). In material coordinates there are two possible normal modes for propagation in each direction, + and -z. These modes are not coupled to one another and correspond to polarization perpendicular and parallel to the fiber direction, respectively. Using the transmission line analogy [2] the response to the normal modes can be written in material coordinates as follows.

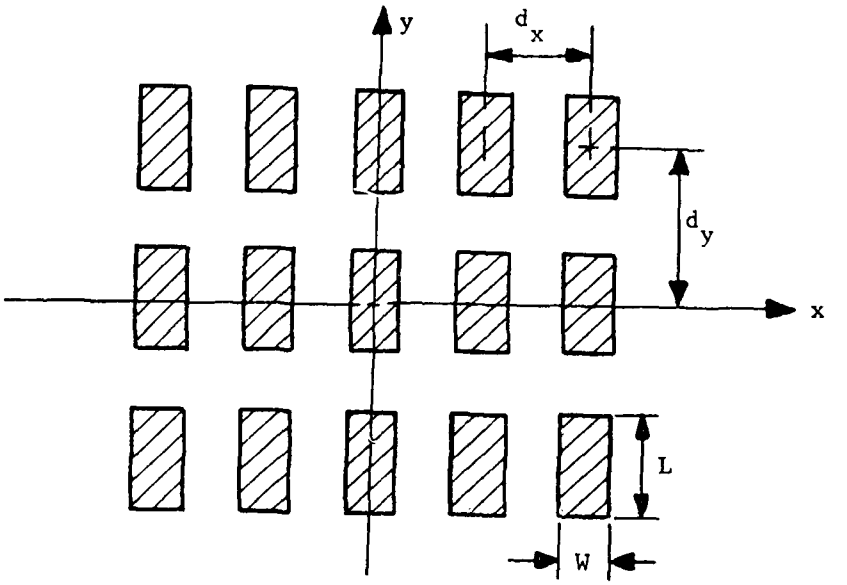

(a) Front View

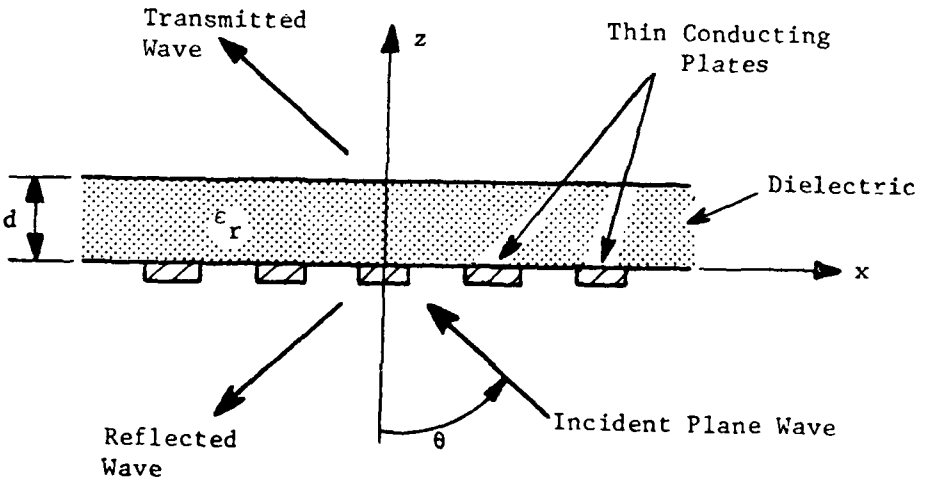

(b) Top View

Figure 19. Model Consisting of an Infinite Periodic Array of Thin Conducting Plates on a Dielectric Sheet. (After Bodnar [16])

For $\vec{E}$ parallel to the fiber direction (ζ_1)

$$\begin{bmatrix} E_{\zeta_1}(\zeta_3) \\ H_{\zeta_2}(\zeta_3) \end{bmatrix} = \begin{bmatrix} \cosh\theta_1 & \eta_1 \sinh\theta_1 \\ \frac{1}{\eta_1}\sinh\theta_1 & \cosh\theta_1 \end{bmatrix} \begin{bmatrix} E_{\zeta_1}(\zeta_3 + t) \\ H_{\zeta_2}(\zeta_3 + t) \end{bmatrix} \tag{62}$$

where

$$\theta_1 = \omega\sqrt{\mu_o \hat{\varepsilon}_{11}}\ t = k_1 t$$

$$\eta_1 = \sqrt{\frac{\mu_o}{\hat{\varepsilon}_{11}}}\ .$$

For $\vec{E}$ perpendicular to the fiber direction but parallel to the plane of the sample (ζ_2)

$$\begin{bmatrix} E_{\zeta_2}(\zeta_3) \\ -H_{\zeta_1}(\zeta_3) \end{bmatrix} = \begin{bmatrix} \cosh\theta_2 & \eta_2 \sinh\theta_2 \\ \frac{1}{\eta_2}\sinh\theta_2 & \cosh\theta_2 \end{bmatrix} \begin{bmatrix} E_{\zeta_2}(\zeta_3 + d) \\ -H_{\zeta_1}(\zeta_3 + d) \end{bmatrix}$$

where $\theta_2 = \omega\sqrt{\mu_o \hat{\varepsilon}_{22}}\ t = k_2 t$

$$\eta_2 = \sqrt{\frac{\mu_o}{\hat{\varepsilon}_{22}}}$$

E_{ζ_1}, H_{ζ_2}, E_{ζ_2}, H_{ζ_1} are components of a single arbitrarily polarized plane wave. It is convenient to collect these terms into a single 4-port matrix equation relating tangential fields at input and output interfaces. E and H terms are slightly rearranged in the new matrix. Note, there is no coupling between the ζ_1 and ζ_2 polarizations.

$$\begin{bmatrix} E_{\zeta_1}(\zeta_3) \\ E_{\zeta_2}(\zeta_3) \\ H_{\zeta_2}(\zeta_3) \\ -H_{\zeta_1}(\zeta_3) \end{bmatrix} = \left[\begin{array}{c|c|c|c} \cosh\theta_1 & 0 & \eta_1\sinh\theta_1 & 0 \\ \hline 0 & \cosh\theta_2 & 0 & \eta_2\sinh\theta_2 \\ \hline \frac{1}{\eta_1}\sinh\theta_1 & 0 & \cosh\theta_1 & 0 \\ \hline 0 & \frac{1}{\eta_2}\sinh\theta_2 & 0 & \cosh\theta_2 \end{array}\right] \begin{bmatrix} E_{\zeta_1}(\zeta_3 + t) \\ E_{\zeta_2}(\zeta_3 + t) \\ H_{\zeta_2}(\zeta_3 + t) \\ -H_{\zeta_1}(\zeta_3 + t) \end{bmatrix} \tag{63}$$

To transform from components expressed in material coordinates to those in propagation coordinates, it can be seen from the geometry of Figure 16 that

$$A_{\zeta_1} = A_x \cos\phi + A_y \sin\phi$$
$$A_{\zeta_2} = -A_x \sin\phi + A_y \cos\phi \tag{64}$$

where A represents either an electric or magnetic field component. Substituting from equation (64) into equation (63) yields the following equation:

$$\begin{bmatrix} E_{i1} \\ E_{i2} \\ H_{i1} \\ H_{i2} \end{bmatrix} = \begin{bmatrix} \cosh\theta_1 & 0 & \eta_1 \sinh\theta_1 & 0 \\ 0 & \cosh\theta_2 & 0 & \eta_2 \sinh\theta_2 \\ \frac{\sinh\theta_1}{\eta_1} & 0 & \cosh\theta_1 & 0 \\ 0 & \frac{\sinh\theta_2}{\eta_2} & 0 & \cosh\theta_2 \end{bmatrix} \begin{bmatrix} E_{o1} \\ E_{o2} \\ H_{o1} \\ H_{o2} \end{bmatrix} \tag{65}$$

where

$$E_{i1} = E_x(z)\cos\phi + E_y(z)\sin\phi$$
$$E_{i2} = -E_x(z)\sin\phi + E_y(z)\cos\phi$$
$$H_{i1} = -H_x(z)\sin\phi + H_y(z)\cos\phi$$
$$H_{i2} = -H_x(z)\cos\phi - H_y(z)\sin\phi$$
$$E_{o1} = E_x(z+t)\cos\phi + E_y(z+t)\sin\phi$$
$$E_{o2} = -E_x(z+t)\sin\phi + E_y(z+t)\cos\phi$$
$$H_{o1} = -H_x(z+t)\sin\phi + H_y(z+t)\cos\phi$$
$$H_{o2} = -H_x(z+t)\cos\phi - H_y(z+t)\sin\phi.$$

Algebraically manipulating equation (65) leads to equation (66) given below.

$$\begin{bmatrix} E_x(z) \\ E_y(z) \\ H_y(z) \\ -H_x(z) \end{bmatrix} = \begin{bmatrix} A_{11} & A_{12} & B_{11} & B_{12} \\ A_{21} & A_{22} & B_{21} & B_{22} \\ C_{11} & C_{12} & D_{11} & D_{12} \\ C_{21} & C_{22} & D_{21} & D_{22} \end{bmatrix} \begin{bmatrix} E_x(z+t) \\ E_y(z+t) \\ H_y(z+t) \\ -H_x(z+t) \end{bmatrix} \tag{66}$$

where

$$A_{11} = D_{11} = \cosh\Theta_1 \cos^2\phi + \cosh\Theta_2 \sin^2\phi$$

$$A_{22} = D_{22} = \cosh\Theta_1 \sin^2\phi + \cosh\Theta_2 \cos^2\phi$$

$$A_{12} = A_{21} = D_{12} = D_{21} = \sin\phi \cos\phi (\cosh\Theta_1 - \cosh\Theta_2)$$

$$B_{11} = \eta_1 \sinh\Theta_1 \cos^2\phi + \eta_2 \sinh\Theta_2 \sin^2\phi$$

$$B_{22} = \eta_1 \sinh\Theta_1 \sin^2\phi + \eta_2 \sinh\Theta_2 \cos^2\phi$$

$$C_{11} = \frac{1}{\eta_1} \sinh\Theta_1 \cos^2\phi + \frac{1}{\eta_2} \sinh\Theta_2 \sin^2\phi$$

$$C_{22} = \frac{1}{\eta_1} \sinh\Theta_1 \sin^2\phi + \frac{1}{\eta_2} \sinh\Theta_2 \cos^2\phi$$

$$B_{12} = B_{21} = \sin\phi \cos\phi (\eta_1 \sinh\Theta_1 - \eta_2 \sinh\Theta_2)$$

$$C_{12} = C_{21} = \sin\phi \cos\phi (\frac{1}{\eta_1} \sinh\Theta_1 - \frac{1}{\eta_2} \sinh\Theta_2).$$

Other quantities have been defined earlier. Notice that x and y polarizations are coupled unless $\phi = 0°$ or $90°$. Thus, except for these two special cases an x-polarized incident wave will produce both x and y polarized reflected and transmitted waves.

A still more condensed equation results if matrix notation is further exploited.

$$\begin{bmatrix} \vec{E}_t(z) \\ \vec{H}_t(z) \end{bmatrix} = \begin{bmatrix} \overleftrightarrow{A} & \overleftrightarrow{B} \\ \overleftrightarrow{C} & \overleftrightarrow{D} \end{bmatrix} \begin{bmatrix} \vec{E}_t(z+t) \\ \vec{H}_t(z+t) \end{bmatrix} \tag{67}$$

where

$$\vec{E}_t(\cdot) = \begin{bmatrix} E_x(\cdot) \\ E_y(\cdot) \end{bmatrix} = \text{Transverse Components of } \vec{E} \text{ at either } z \text{ or } z+t$$

$$\vec{H}_t(\cdot) = \begin{bmatrix} H_y(\cdot) \\ -H_x(\cdot) \end{bmatrix} = \text{Transverse Components of H at either } z \text{ or } z+t$$

and $$\overleftrightarrow{A} = \begin{bmatrix} A_{11} & A_{12} \\ A_{21} & A_{22} \end{bmatrix}$$

$$\overleftrightarrow{B} = \begin{bmatrix} B_{11} & B_{12} \\ B_{21} & B_{22} \end{bmatrix}, \text{ etc.}$$

and A_{ij}, B_{ij}, C_{ij}, D_{ij}; coefficients were defined above. This 4-port structure is illustrated schematically in Figure 20.

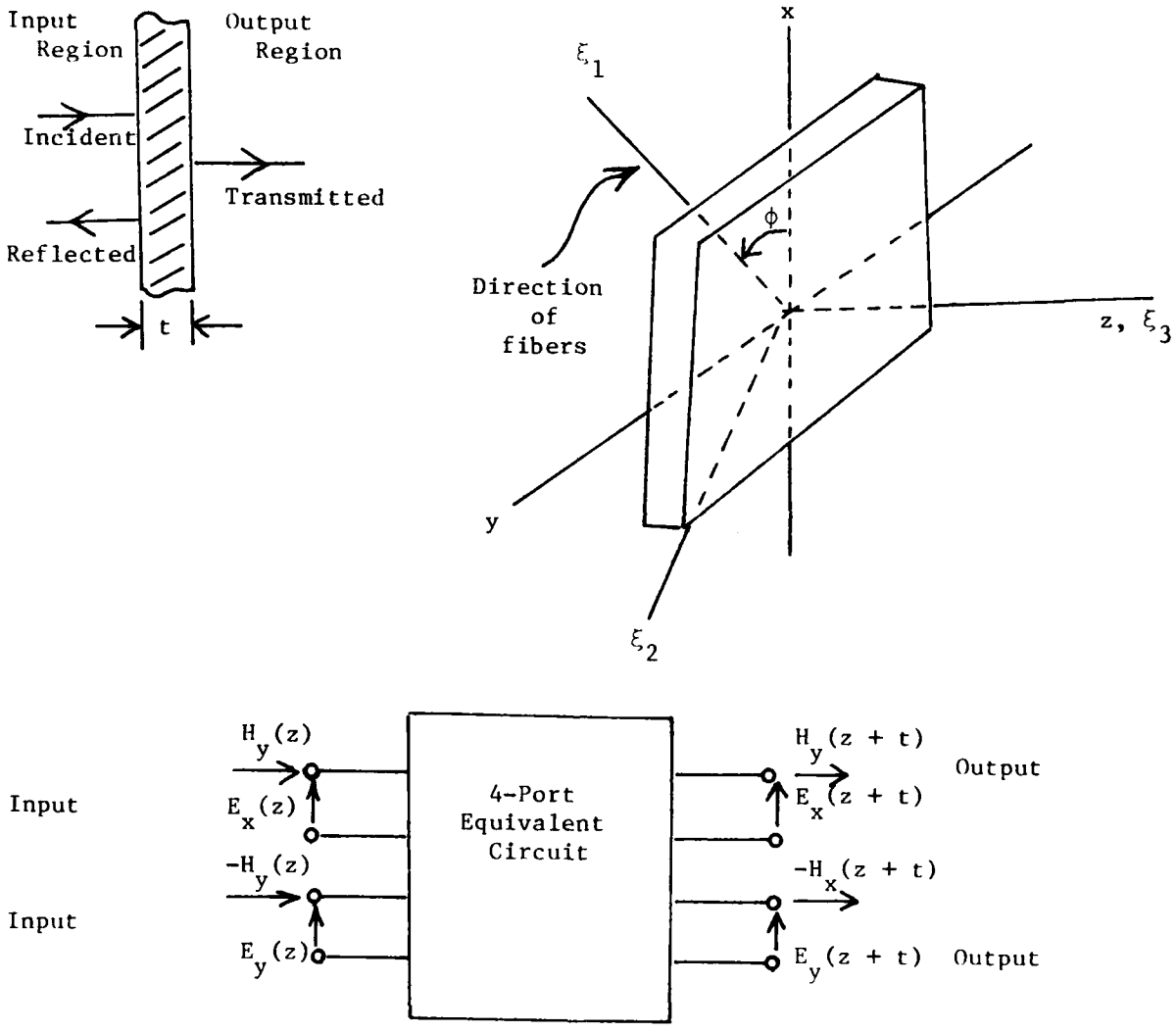

Figure 20. Anisotropic Shields

5.4 Multilayer Samples with Normally Incident, Arbitrarily Polarized Plane Waves

To analyze multilayer structures, construct $\begin{bmatrix} \overleftrightarrow{A} & \overleftrightarrow{B} \\ \overleftrightarrow{C} & \overleftrightarrow{D} \end{bmatrix}$ for each layer taking into account the different ϕ and $\overleftrightarrow{\epsilon}$ for each layer. Obtain the overall ABCD matrix as the product of the matrices for the individual layers. Thus, for a 90°, 45°, 90° multilayer sample

$$\begin{bmatrix} \overleftrightarrow{A} & \overleftrightarrow{B} \\ \overleftrightarrow{C} & \overleftrightarrow{D} \end{bmatrix} = \begin{bmatrix} \overleftrightarrow{A}_{90°} & \overleftrightarrow{B}_{90°} \\ \overleftrightarrow{C}_{90°} & \overleftrightarrow{D}_{90°} \end{bmatrix} \begin{bmatrix} \overleftrightarrow{A}_{45°} & \overleftrightarrow{B}_{45°} \\ \overleftrightarrow{C}_{45°} & \overleftrightarrow{D}_{45°} \end{bmatrix} \begin{bmatrix} \overleftrightarrow{A}_{90°} & \overleftrightarrow{B}_{90°} \\ \overleftrightarrow{C}_{90°} & \overleftrightarrow{D}_{90°} \end{bmatrix}. \tag{68}$$

The resulting ABDC matrix relates the "total" (i.e., sum of incident and reflected) fields at the input side of the sample to the corresponding quantities on the output side. Most often the desired end result of such analysis is various ratios of traveling wave (not "total") fields. To facilitate calculations such as determining power reflected, power transmitted, power converted from one polarization to another, etc., it is convenient after the overall ABCD matrix is computed to convert to scattering parameters [4]. Scattering parameters provide direct relationships between the traveling wave quantities. Clearly, scattering parameters or their transmission counterpart could be used to describe each layer and then combined to provide the overall multilayer matrix. However, the determination of the overall ABCD matrix and then its conversion to scattering parameters is computationally much more efficient in the class of problems being considered.

5.5 Scattering Matrix for a Multilayer Anisotropic Structure with Normally Incident, Arbitrarily Polarized Plane Waves

Either normalized or unnormalized scattering parameters [4] may be used. In many cases normalized parameters are a distinct advantage. At this point there is little advantage to be gained from normalization and some danger of confusion arising from the normalization process. Therefore, unnormalized scattering parameters are used.

Let the fields on the input side of the sample be expressed as follows:

$$\begin{cases} E_x(z) = E_{xi}(z) + E_{xr}(z) \\ E_y(z) = E_{yi}(z) + E_{yr}(z) \\ H_y(z) = H_{yi}(z) + H_{yr}(z) = \dfrac{1}{\eta_s}\,[E_{xi}(z) - E_{xr}(z)] \\ -H_x(z) = -[H_{xi}(z) + H_{xr}(z)] = \dfrac{+1}{\eta_s}[E_{yi}(z) - E_{yr}(z)] \end{cases} \tag{69}$$

where η_s = intrinsic impedance of input medium and the subscript i refers to incident traveling wave components while r refers to reflected or reverse traveling wave components.

Similarly, fields on the output side of the sample are given in equation (70). Note, as is conventional in scattering analysis "incident waves" travel towards the sample while "scattered or reflected waves" travel away from the sample. This means that incident waves on opposite sides of the sample travel in opposite directions.

$$\begin{cases} E_x(z+t) = E_{xi}(z+t) + E_{xr}(z+t) \\ E_y(z+t) = E_{yi}(z+t) + E_{yr}(z+t) \\ H_y(z+t) = H_{yi}(z+t) + H_{yr}(z+t) = \frac{-1}{\eta_3}[E_{xi}(z+t) - E_{xr}(z+t)] \\ -H_x(z+t) = -[H_{xi}(z+t) + H_{xr}(z+t)] = \frac{-1}{\eta_3}[E_{yi}(z+t) - E_{yr}(z+t)] \end{cases} \tag{70}$$

where η_3 = intrinsic impedance of output medium.

If there are no sources on the output side of the sample, the incident signals from that side will be zero, i.e., $E_{yi}(z+t) = E_{xi}(z+t) = 0$. It is assumed that this is true in the following analysis. Substituting equations (69) and (70) into equation (67) and solving for the scattered or reflected components in terms of the nonzero incident components yields the following relationship. Note that since $E_{yi}(z+t) = E_{xi}(z+t) = 0$, only the first two columns of the scattering matrix are required for this analysis.

$$\begin{bmatrix} E_{xr}(z) \\ E_{yr}(z) \\ E_{xr}(z+t \\ E_{yr}(z+t) \end{bmatrix} = \begin{bmatrix} S_{11} & S_{12} & S_{13} & S_{14} \\ S_{21} & S_{22} & S_{23} & S_{24} \\ S_{31} & S_{32} & S_{33} & S_{34} \\ S_{41} & S_{42} & S_{43} & S_{44} \end{bmatrix} \begin{bmatrix} E_{xi}(z) \\ E_{yi}(z) \\ 0 \\ 0 \end{bmatrix} \tag{71}$$

where

$$S_{41} = \frac{2}{\Delta}\left[A_{21} + \frac{B_{21}}{\eta_3} - \eta_s C_{21} - \frac{\eta_s}{\eta_3} D_{21}\right]$$

$$S_{42} = \frac{-2}{\Delta}\left[A_{11} + \frac{B_{11}}{\eta_3} + \eta_s C_{11} + \frac{\eta_s}{\eta_3} D_{11}\right]$$

$$S_{31} = \frac{-2}{\Delta}\left[A_{22} - \frac{B_{22}}{\eta_3} - \eta_s C_{22} + \frac{\eta_s}{\eta_3} D_{22}\right]$$

$$S_{32} = \frac{2}{\Delta}\left[A_{12} - \frac{B_{12}}{\eta_3} + \eta_s C_{12} - \frac{\eta_s}{\eta_3} D_{12}\right]$$

$$S_{21} = \left[\left(A_{21} + \frac{B_{21}}{\eta_3}\right) S_{31} + \left(A_{22} + \frac{B_{22}}{\eta_3}\right) S_{41}\right]$$

$$S_{22} = \left[-1 + \left(A_{21} + \frac{B_{21}}{\eta_3}\right) S_{32} + \left(A_{22} + \frac{B_{22}}{\eta_3}\right) S_{42}\right]$$

$$S_{11} = \left[-1 + \left(A_{11} + \frac{B_{11}}{\eta_3}\right) S_{31} + \left(A_{12} + \frac{B_{12}}{\eta_3}\right) S_{41}\right]$$

$$S_{12} = \left[\left(A_{11} + \frac{B_{11}}{\eta_3}\right) S_{32} + \left(A_{12} + \frac{B_{12}}{\eta_3}\right) S_{42}\right]$$

$$\Delta = \left[\left(A_{12} - \frac{B_{12}}{\eta_3} + \eta_s C_{12} - \frac{\eta_s}{\eta_3} D_{12}\right)\left(A_{21} + \frac{B_{21}}{\eta_3} - \eta_s C_{21} - \frac{\eta_s}{\eta_3} D_{21}\right)\right.$$
$$\left. -\left(A_{11} + \frac{B_{11}}{\eta_3} + \eta_s C_{11} + \frac{\eta_s}{\eta_3} D_{11}\right)\left(A_{22} - \frac{B_{22}}{\eta_3} - \eta_s C_{22} + \frac{\eta_s}{\eta_3} D_{22}\right)\right] .$$

Equation (71) can be used to calculate the quantities of interest in electromagnetic shielding problems. The procedure is to first calculate the total 4-port ABCD parameters for the multilayer sample, as indicated in Section 5.3. The values of A_{ij}, B_{ij}, C_{ij}, D_{ij} obtained are used in equation (71) to determine the overall scattering parameters for the multilayer sample. Figure 21 and 22 illustrate shielding effectiveness calculated for some single-layer and multilayer graphite epoxy shields. The value of ε_r' is not critical for the values of conductivity utilized. Indeed varying ε_r' from 1 to about 100 has no noticeable effect on the shielding effectiveness. Figure 21 illustrates the effect on shielding effectiveness of varying polarization of the wave incident on a single anisotropic layer. Data is plotted for polarization parallel to the fiber direction ($\phi = 0°$), perpendicular to the fiber direction ($\phi = 90°$) and inclined at 45° to the fiber direction ($\phi = 45°$). As would be expected, much larger attenuation is experienced when the wave is polarized parallel to the fibers. Figure 22 illustrates shielding effectiveness for 4-layer (0°, $\pm$ 45°, 90°) and 7-layer (0°, $\pm$ 45°, 90°, $\pm$ 45°, 0°) structures. The incident wave in each case is polarized parallel to the fiber direction of the first layer.

5.6 Scattering Matrix for a Multilayer Anisotropic Shield with Incident Plane Wave of Arbitrary Polarization and Angle of Incidence

Consider a shield consisting of planar, homogeneous, anisotropic layers arranged as shown in Figure 23. Each layer is assumed uniaxial with the optic axis parallel to the xy plane. Input and output regions are homogeneous and isotropic with relative permittivities ε'' and ε', respectively. A plane wave of radian frequency ω is incident from the region $z < 0$ on the shield with angle of incidence ϕ_o.

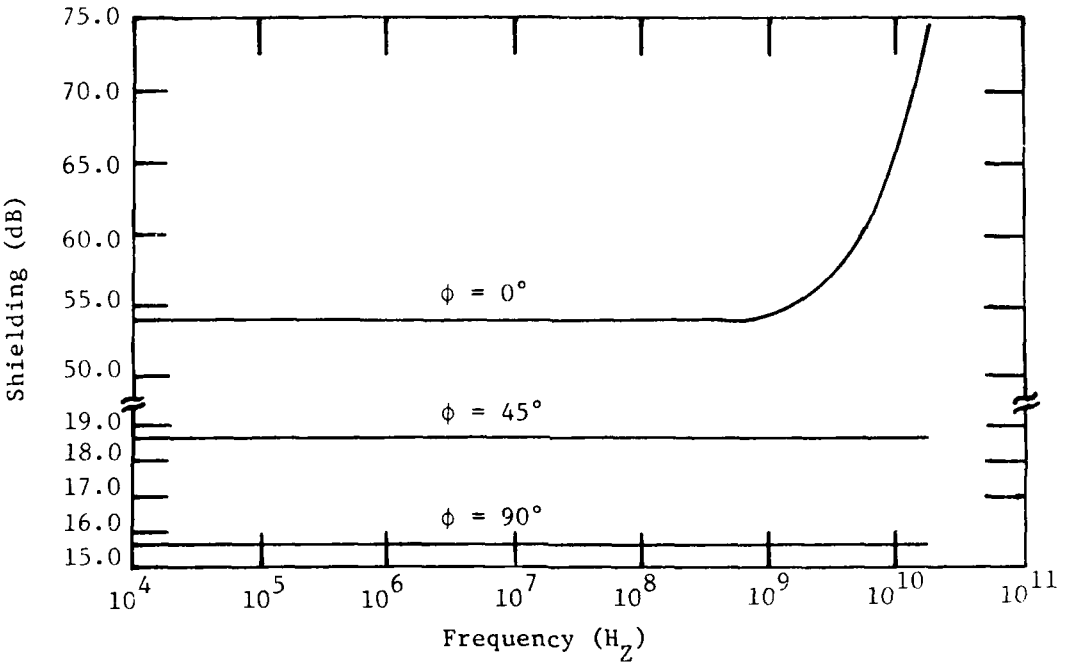

Figure 21. Shielding effectiveness of a single layer anisotropic shield for various fiber orientations. A plane wave polarized in the $\phi = 0°$ direction is normally incident on the input side of the shield, shield parameters are $t = .00525$ inches, $\sigma = 2 \times 10^4$ mhos/m, $\sigma_2 = 2 \times 10^2$ mhos/m, $\varepsilon_{r1} = \varepsilon_{r2} = 3$.

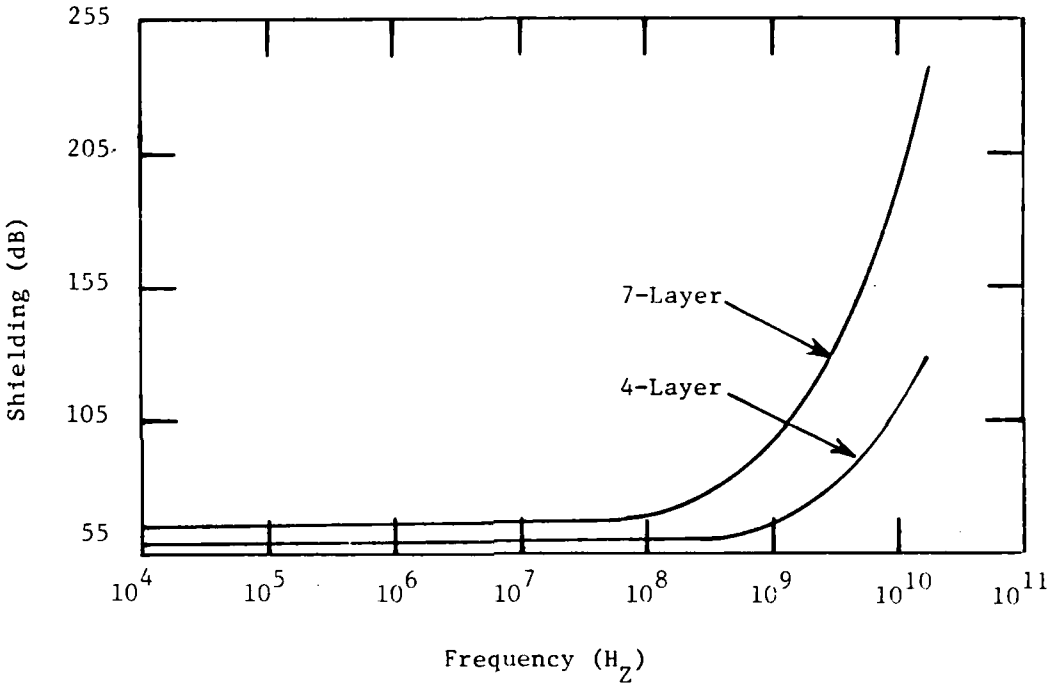

Figure 22. Shielding effectiveness of 4-layer and 7-layer anisotropic shields. Fiber orientations for 4-layer shield are (0°, ± 45°, 90°); for 7-layer shield are (0°, ± 45°, 90°, ± 45°, 0°). Each layer has t = .00525 inches, σ_1 = 2 x 10^4 mhos/m, σ_2 = 2 x 10^2 mhos/m, $\varepsilon_{r1} = \varepsilon_{r2} = 3$.

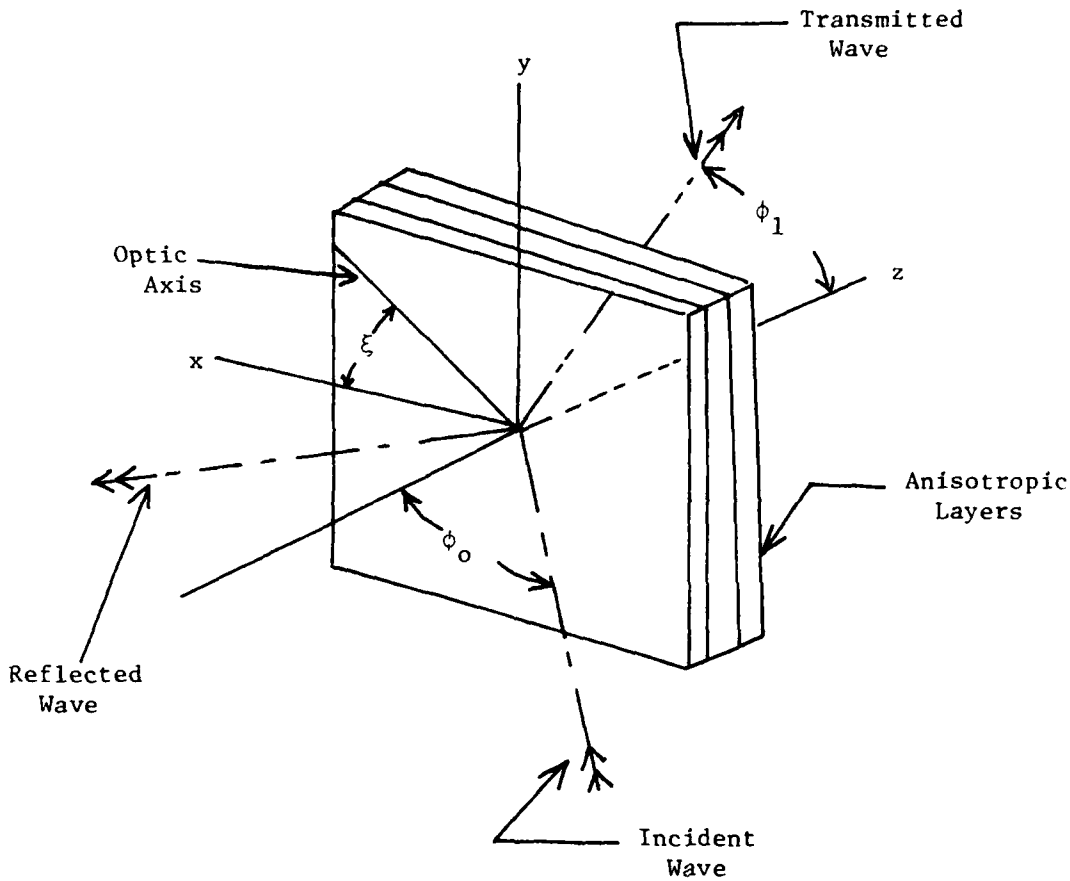

Figure 23. Multilayer Anisotropic Shield with Incident Plane Wave at Arbitrary Angle of Incidence. Shield Infinite in Extent in xy-Plane. Plane of Incidence is the xz-Plane.

To evaluate the shielding provided by this structure, the problem may be stated as follows. Given the parameters of the anisotropic layers of the shield plus the frequency and direction of propagation of the incident wave, determine the reflected and transmitted waves. Using the techniques of Section 5.3 of this report, the above problem reduces to that of determining the transfer matrix of the stratified anisotropic shield for the specified excitation. The folloiwng derivation of the necessary transfer matrix is similar to the optic problem solved by Semenko and Mironov [20].

Within each anisotropic layer, Maxwell's curl equations become

$$\begin{aligned} \nabla \times \vec{E} &= -j\omega\mu_o \vec{H} \\ \nabla \times \vec{H} &= (\overleftrightarrow{\sigma} + \omega\overleftrightarrow{\varepsilon})\vec{E} \end{aligned} \tag{72}$$

where $\overleftrightarrow{\sigma}$ and $\overleftrightarrow{\varepsilon}$ are the matrix representations of the layer conductivity and permittivity, respectively, and unity relative permeability has been assumed.

Eliminating H from (72) yields the wave equation for this type of anisotropic media.

$$\nabla^2\vec{E} = \nabla(\nabla \cdot \vec{E}) - \beta_o^2 \langle\varepsilon\rangle \vec{E} \tag{73}$$

where

$$\beta_o^2 = \frac{\omega^2}{c^2}$$

$$\langle\varepsilon\rangle = \overleftrightarrow{\varepsilon}_r - j\,\frac{1}{\omega\varepsilon_o}\,\overleftrightarrow{\sigma} = \text{Complex permittivity}$$

$\overleftrightarrow{\varepsilon}_r$ = Matrix representation of relative permittivity

ε_o = Permittivity of free space, and

$\overleftrightarrow{\varepsilon}_r$ and $\overleftrightarrow{\sigma}$ are assumed to have the same optic axis.

Based on the assumption that each layer is uniaxial and recognizing that the matrix representation of the complex permittivity is symmetric [21], $\langle\varepsilon\rangle$ can be written in the following form.

$$\langle\varepsilon\rangle = \begin{array}{c|ccc} & x & y & z \\ \hline x & \varepsilon_{11} & \varepsilon_{12} & 0 \\ y & \varepsilon_{12} & \varepsilon_{22} & 0 \\ z & 0 & 0 & \varepsilon_{33} \end{array} \tag{74}$$

where

$$\varepsilon_{11} = \varepsilon_1 \cos^2 \zeta + \varepsilon_2 \sin^2 \zeta$$

$$\varepsilon_{22} = \varepsilon_1 \sin^2 \zeta + \varepsilon_2 \cos^2 \zeta$$

$$\varepsilon_{12} = (\varepsilon_2 - \varepsilon_1) \sin \zeta \cos \zeta$$

$$\varepsilon_{33} = \varepsilon_2$$

ε_1, ε_2 are the principal axis complex permittivities

ζ is the angle between the x-axis and the optic axis.

The tangential field components and their first derivatives are continuous across any interface parallel to the xy plane. Thus,

$$\frac{\partial}{\partial y} = 0$$

$$\frac{\partial}{\partial x} = -j\beta_o\sqrt{\varepsilon_{or}} \sin \phi_o = \text{constant} = -jk_x \tag{75}$$

where ε_{or} is the relative permittivity of the input medium.

Substituting (74) and (75) into (73) yields for the z-component of E

$$E_z = \frac{-jk_x}{f} D_z E_x \tag{76}$$

where

$$k_x = \beta_o\sqrt{\varepsilon_o} \sin \phi_o$$

$$D_z = d/dz$$

$$f = \beta_o^2 \varepsilon_{33} - k_x^2 .$$

The tangential field components E_x and E_y must satisfy the following homogeneous matrix equation.

$$\begin{bmatrix} 0 \\ 0 \end{bmatrix} = \begin{bmatrix} \beta_o^2\varepsilon_{11} + \left(1 + \frac{k_x^2}{f}\right)D_z^2 & \beta_o^2\varepsilon_{12} \\ \beta_o^2\varepsilon_{12} & \beta_o^2\varepsilon_{22} - k_x^2 + D_z^2 \end{bmatrix} \begin{bmatrix} E_x \\ E_y \end{bmatrix} \tag{77}$$

Equation (77) is a system of two second-order ordinary differential equations. Solutions of the form $\exp\{-jk_z z\}$ are sought. Thus, $D_z = -jk_z$ and after simplification (77) becomes

$$\begin{bmatrix} 0 \\ 0 \end{bmatrix} = \begin{bmatrix} \beta_o^2\varepsilon_{11} - k_z^2 \dfrac{\beta_o^2\varepsilon_{33}}{f} & \beta_o^2\varepsilon_{12} \\ \beta_o^2\varepsilon_{12} & \beta_o^2\varepsilon_{22} - k_x^2 - k_z^2 \end{bmatrix} \begin{bmatrix} E_x \\ E_y \end{bmatrix} \tag{78}$$

If (78) is to have a non-trivial solution, the determinant of the coefficient matrix must be zero. This constraint yeilds Fresnel's equation and permits the solution for the z-component of the wave vector, k_z. After some algebraic manipulation, the following quadratic in k_z^2 is obtained.

$$0 = \left(k_z^2\right)^2 - \left(k_z^2\right)\left(f\,\frac{\varepsilon_{11}}{\varepsilon_{33}} + g\right) + \frac{f}{\varepsilon_{33}}\left(g\varepsilon_{11} - \beta_o^2\varepsilon_{12}^2\right) \tag{79}$$

where

$$g = \beta_o^2\varepsilon_{22} - k_x^2 .$$

Solving for k_z^2 yields

$$k_z^2 = \frac{1}{2}\left\{\left(f\,\frac{\varepsilon_{11}}{\varepsilon_{33}} + g\right) \pm \sqrt{\left(f\,\frac{\varepsilon_{11}}{\varepsilon_{33}} - g\right)^2 + 4f\beta_o^2\,\frac{\varepsilon_{12}^2}{\varepsilon_{33}}}\right\} \tag{80}$$

$$= \frac{1}{2}\,(C \pm R).$$

Denoting the four admissible solutions (80) as k_i for i = 1, 2, 3, 4 yields

$$\begin{aligned} k_1 &= \frac{1}{4}\sqrt{C + R} = -k_3 \\ k_2 &= \frac{1}{4}\sqrt{C - R} = -k_4 \end{aligned} \tag{81}$$

The general solutions for E_x and E_y can now be obtained from (73) and are of the following form.

$$\begin{aligned} E_x(z) &= \sum_{i=1}^{4} \gamma_i q_i \exp\{-jk_i z\} \\ E_y(z) &= \sum_{i=1}^{4} q_i \exp\{-jk_i z\} \end{aligned} \tag{82}$$

where

$$\gamma_1 = \gamma_3 = \frac{f\,\frac{\varepsilon_{12}}{\varepsilon_{33}}}{(k_1)^2 - f\,\frac{\varepsilon_{11}}{\varepsilon_{33}}}$$

$$\gamma_2 = \gamma_4 = \frac{f\,\frac{\varepsilon_{12}}{\varepsilon_{33}}}{(k_2)^2 - f\,\frac{\varepsilon_{11}}{\varepsilon_{33}}}$$

Likewise, the tangential components of the magnetic field are of the form:

$$H_x(z) = \frac{-1}{\omega\mu} \sum_{i=1}^{4} q_i\, k_i\, \exp\{-jk_i z\}$$

$$H_y(z) = \frac{\beta_o^2 \varepsilon_{33}}{f\omega\mu} \sum_{i=1}^{4} \gamma_i\, q_i\, k_i\, \exp\{-jk_i z\} \quad . \tag{83}$$

The constants $q_i (i = 1, 2, 3, 4)$ can be evaluated by applying boundary conditions to the tangential components of the electric and magnetic fields.

Using (82) and (83), the tangential field components may be expressed in matrix form as follows.

$$Q(z) = \Gamma\, \varepsilon(z) Q \tag{84}$$

where

$$Q(z) = \begin{bmatrix} E_x(z) \\ E_y(z) \\ H_y(z) \\ H_x(z) \end{bmatrix}$$

$$Q = \begin{bmatrix} q_1 \\ q_2 \\ q_3 \\ q_4 \end{bmatrix}$$

$$\varepsilon(z) = \begin{bmatrix} \exp(-jk_1 z) & 0 & 0 & 0 \\ 0 & \exp(-jk_2 z) & 0 & 0 \\ 0 & 0 & \exp(-jk_3 z) & 0 \\ 0 & 0 & 0 & \exp(-jk_4 z) \end{bmatrix}$$

$$\Gamma = \begin{bmatrix} \gamma_1 & \gamma_2 & \gamma_3 & \gamma_4 \\ 1 & 1 & 1 & 1 \\ \rho_1\gamma_1 k_1 & \rho_1\gamma_2 k_2 & \rho_1\gamma_3 k_3 & \rho_1 k_4\gamma_4 \\ \rho_2 k_1 & \rho_2 k_2 & \rho_2 k_3 & \rho_2 k_4 \end{bmatrix}$$

$$\rho_1 = \frac{\beta_o^2 \varepsilon_{33}}{f\omega\mu_o}$$

$$\rho_2 = \frac{1}{\omega\mu_o} .$$

Likewise, the inverse of the matrix is

$$\Gamma^{-1} = \frac{1}{2\Delta} \begin{bmatrix} 1 & -\gamma_2 & 1/\rho_1 k_1 & -\gamma_2/\rho_2 k_1 \\ -1 & \gamma_1 & -1/\rho_1 k_2 & \gamma_1/\rho_2 k_2 \\ 1 & -\gamma_2 & -1/\rho_1 k_1 & \gamma_2/\rho_2 k_1 \\ -1 & \gamma_1 & 1/\rho_1 k_2 & -\gamma_1/\rho_2 k_2 \end{bmatrix}$$

where $\Delta = \gamma_1 - \gamma_2$

and k_1 and k_2 are the two solutions to Fresnel's equation

$$\gamma_i = \left. \frac{-\varepsilon_{12}}{\varepsilon_{11} - \frac{\varepsilon_{33}}{f} k_z^2} \right|_{k_z = k_i} \qquad \text{for } i = 1, 2$$

Consider the layered shield depicted in Figure 24. In each region the tangential field

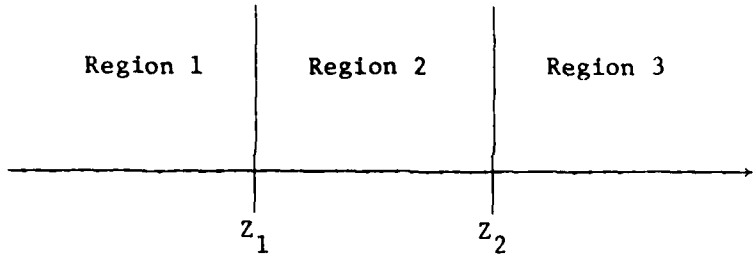

Figure 24. Layered Anisotropic Shield

components are given by (84)

$$\begin{aligned} &\text{Region 1.} \quad Q(z) = \Gamma_1 \varepsilon_1(z) Q_1 \qquad z < Z_1 \\ &\text{Region 2.} \quad Q(z) = \Gamma_2 \varepsilon_2(z) Q_2 \qquad Z_1 < z < Z_2 \\ &\text{Region 3.} \quad Q(z) = \Gamma_3 \varepsilon_3(z) Q_3 \qquad z > Z_2 \end{aligned} \tag{85}$$

Column vectors Q_1, Q_2 are chosen such that the tangential fields $Q(z)$ are continuous throughout the three regions.

$$Q(Z_1) = \Gamma_1 \varepsilon_1(Z_1) Q_1 = \Gamma_2 \varepsilon_2(Z_1) Q_2 \tag{86A}$$

$$Q(Z_2) = \Gamma_2 \varepsilon_2(Z_2) Q_2 = \Gamma_3 \varepsilon_3(Z_2) Q_3 \tag{86B}$$

From (86B)

$$Q_2 = [\Gamma_2 \varepsilon_2(Z_2)]^{-1} Q(Z_2) \ . \tag{87}$$

Substituting (87) into (86A) yields

$$\begin{aligned} Q(Z_1) &= \Gamma_2 \varepsilon_2(Z_1) [\Gamma_2 \varepsilon_2(Z_1)]^{-1} Q(Z_2) \\ &= \Gamma_2 [\varepsilon_2(Z_1) \varepsilon_2^{-1}(Z_2)] \Gamma_2^{-1} Q(Z_2) \\ &= [\Gamma_2 \varepsilon_2^{-1}(Z_2 - Z_1) \Gamma_2^{-1}] Q(Z_2) \end{aligned} \tag{88}$$

Equation (88) specifies the transfer matrix (note that this transfer matrix is for output variables in terms of input variables) for the region $Z_1 < z < Z_2$. The quantity $Z_2 - Z_1$ is simply the thickness of the region. For

a system of N layers, each of thickness d_j, the overall transfer matrix is simply the product of the transfer matrices for the individual layers.

$$T = \prod_{j=1}^{N} \left[\Gamma_j \, \varepsilon^{-1}(d_j) \Gamma_j^{-1} \right] \tag{89}$$

From equation (89) the transfer matrix of a single anisotropic layer of thickness d can be written in the following form.

$$\overleftrightarrow{T} = \begin{bmatrix} A_{11} & A_{12} & B_{11} & B_{12} \\ A_{21} & A_{22} & B_{21} & B_{22} \\ C_{11} & C_{12} & D_{11} & D_{12} \\ C_{21} & C_{22} & D_{21} & D_{22} \end{bmatrix} \tag{90}$$

where

$$A_{11} = D_{11} = \frac{1}{\cos^2 \hat{U}} \left[\cos^2 \hat{\phi} \cos^2 \zeta \cosh \hat{\theta}_1 + \sin^2 \zeta \cosh \hat{\theta}_2 \right]$$

$$A_{22} = D_{22} = \frac{1}{\cos^2 \hat{U}} \left[\sin^2 \zeta \cosh \hat{\theta}_1 + \cos^2 \hat{\phi} \cos^2 \zeta \cosh \hat{\theta}_2 \right]$$

$$A_{21} = D_{12} = \frac{1}{\cos^2 \hat{U}} \sin \zeta \cos \zeta \left[\cosh \hat{\theta}_1 - \cosh \hat{\theta}_2 \right]$$

$$A_{12} = D_{21} = \cos^2 \hat{\phi} \, A_{21}$$

$$B_{11} = \frac{1}{\cos^2 \hat{U}} \left[\cos^4 \hat{\phi} \, \frac{\hat{\eta}_1}{\cos \hat{V}} \cos^2 \zeta \sinh \hat{\theta}_1 + \hat{\eta}_2 \cos \hat{\phi} \sin^2 \zeta \sinh \hat{\theta}_2 \right]$$

$$B_{12} = B_{21} = \frac{1}{\cos^2 \hat{U}} \left[\cos^2 \hat{\phi} \, \frac{\hat{\eta}_1}{\cos \hat{V}} \sinh \hat{\theta}_1 - \hat{\eta}_2 \cos \hat{\phi} \sinh \hat{\theta}_2 \right] \sin \zeta \cos \zeta$$

$$B_{22} = \frac{1}{\cos^2 \hat{U}} \left[\frac{\hat{\eta}_1}{\cos \hat{V}} \sin^2 \zeta \sinh \hat{\theta}_1 + \hat{\eta}_2 \cos \hat{\phi} \cos^2 \zeta \sinh \hat{\theta}_2 \right]$$

$$C_{11} = \frac{1}{\cos^2 \hat{U}} \left[\frac{\cos \hat{V}}{\hat{\eta}_1} \cos^2 \zeta \sinh \hat{\theta}_1 + \frac{1}{\hat{\eta}_2 \cos \hat{\phi}} \sin^2 \zeta \sinh \hat{\theta}_2 \right]$$

$$C_{12} = C_{21} = \frac{1}{\cos^2 \hat{U}} \sin \zeta \cos \zeta \left[\frac{\cos \hat{V}}{\hat{\eta}_1} \sinh \hat{\theta}_1 - \frac{1}{\hat{\eta}_2} \cos \hat{\phi} \sinh \hat{\theta}_2 \right]$$

$$C_{22} = \frac{1}{\cos^2 \hat{U}} \left[\frac{\cos \hat{V}}{\hat{\eta}_1} \sin^2 \zeta \sinh \hat{\theta}_1 + \frac{1}{\hat{\eta}_2} \cos^3 \hat{\phi} \cos^2 \zeta \sinh \hat{\theta}_2 \right]$$

and

$$\hat{\eta}_1 = \sqrt{\frac{\mu_o}{\varepsilon_o}} \frac{\sqrt{\mu_1}}{\sqrt{\varepsilon_1}}$$

$$\hat{\eta}_2 = \sqrt{\frac{\mu_o}{\varepsilon_o}} \frac{\sqrt{\mu_2}}{\sqrt{\varepsilon_2}}$$

$$\cos^2 \hat{\phi} = 1 - \frac{\varepsilon_{or}}{\varepsilon_2} \sin^2 \phi_o$$

$$\cos^2 \hat{U} = 1 - \frac{\varepsilon_{or}}{\varepsilon_2} \sin^2 \phi_o \cos^2 \zeta$$

$$\cos^2 \hat{V} = \cos^2 \hat{U} - \frac{\varepsilon_{or}}{\varepsilon_1} \sin^2 \phi_o \sin^2 \zeta$$

$$\hat{\theta}_1 = jk_1 d$$

$$\hat{\theta}_2 = jk_2 d \ .$$

Scattering parameters and hence reflected and transmitted fields can now be calculated using Equation 71 of Section 5.5 of this report. Equations (90) reduce to Equation (66) of Section 5.3 when the angle of incidence, ϕ_1, is set equal to zero.

6.0 Summary and Conclusions

"ABCD" and "Scattering" matrix analysis techniques for determining shielding effectiveness of isotropic and anisotropic multilayered shields are

presented. These techniques are well-suited to computer implementation. Such programs have been generated and reported on separately.

Given appropriate intrinsic material properties as input, the computer simulations yield surface transfer impedance and shielding effectiveness numbers in excellent agreement with Boeing [6] experimental data. The programs can also be used to infer intrinsic material parameters given measured surface transfer impedance and/or shielding effectiveness data.

From reported measurements on advanced composite materials, it is apparent that the major shielding problem associated with these materials arises from seams and joints. Even in the laboratory under well controlled conditions, it has proven exceptionally difficult to obtain reliable, repeatable joints. Many of the measured results appear erratic (especially in comparing between different measurement schemes) largely due to uncontrollable seam and joint leakage where the composite sample is mated to the measurement system.

REFERENCES

1. Electromagnetic Properties and Effects of Advanced Composite Materials: Measurement and Modeling, RADC-TR-78-156, Phase Report, June 1978.

2. S. A. Schelkunoff, Electromagnetic Waves, D. Van Nostrand (1943).

3. W. E. Lewis and D. G. Pryce, The Application of Matrix Theory to Electrical Engineering, E. & F. N. Spon (London), 1965.

4. L. Weinberg, "Fundamentals of Scattering Matrices," Electro-Technology, July 1967, pp. 55-72.

5. S. Ramo, J. R. Whinnery, and T. Van Duzer, Fields and Waves in Communication Electronics, John Wiley and Sons (1967).

6. D. Strawe, L. Piszker, "Interaction of Advanced Composites with Electromagnetic Pulse (EMP) Environment," AFML-TR-75-14), September 1975, (AD-B011927).

7. J. Moser, "Low-frequency Shielding of a Circular Loop Electromagnetic Field," IEEE Trans. on EMC, Vol. EMC-9, pp. 6-18, March 1967.

8. P. Bannister, "New Theoretical Expressions for Predicting Shielding Effectiveness for the Plane Shield Case," IEEE Trans. on EMC, Vol. EMC-10, pp. 2-7, March 1968.

9. P. Bannister, "Further Notes for Predicting Shielding Effectiveness for the Plane Shield Case," IEEE Trans. on EMC, Vol. EMC-11, pp. 50-53, May 1969.

10. A Technology Plan for Electromagnetic Characteristics of Advanced Composites, RADC-TR-76-206, July 1976.

11. Technique of Microwave Measurements, Edited by C. G. Montgomery, Vol. II, Radiation Laboratory Series, Chapter 10, McGraw-Hill (1947).

12. M. G. Salvadori and M. L. Baron, Numerical Methods in Engineering, Prentice Hall, Inc. (1961).

13. H. J. Carlin and A. B. Giordano, Network Theory: An Introduction to Reciprocal and Nonreciprocal Circuits, Prentice-Hall, Inc. (1964).

14. K. Kurokawa, "Power Waves and the Scattering Matrix," IEEE Trans. MTT, March 1965, pp. 194-203.

15. N. Kuhn, "Simplified Signal Flow Graph Analysis," Microwave Journal, November 1963, pp. 59-66.

16. D. Bodnar, "Electromagnetic Shielding of Structural Foams by Using Internal Conductive Materials," AMMRC TR78-2.

17. N. Marcavitz, Waveguide Handbook, McGraw-Hill, 1951, Chapter 5.

18. C. C. Chen, "Scattering by a Two-Dimensional Periodic Array of Conducting Plates," IEEE Trans. AP, Sept. 1970, pp. 660-665.

19. J. P. Montgomery, "Scattering by an Infinite Periodic Array of Thin Conductors on the Dielectric Sheet," IEEE Trans. AP, January 1975, pp. 70-75.

20. A. I. Semenenko and F. S. Mironov, "Matrix Methods in the Optics of Anisotropic Layered Media," Opt. Spectrosc., Vol. 41, Sept. 1976, pp. 262-265.

21. L. D. Landav and E. M. Lifshitz, Electrodynamics of Continuous Media, Pergamon Press, Oxford, 1960.

APPENDIX A

DERIVATION OF EQUATION (9)

Moser [7] and Bannister [8, 9] have provided an integral equation solution for the shielding effectiveness of the two-loop/infinite flat plate geometry assuming uniform current in the loops. It is assumed that the shield can be neglected. The complete expression for the shielding effectiveness as given by Bannister is shown in equation (A-1).

$$S.\ E._{dB} = 20 \log_{10} \frac{1}{4\mu_r} \left| \frac{\int_0^\infty \frac{\lambda^2}{\tau_o} J_1(\lambda a) \varepsilon^{-\tau_o z} d\lambda}{\int_0^\infty \frac{C\lambda^2 \tau}{\tau_o^2} J_1(\lambda a) \varepsilon^{-\tau_o z - t(\tau - \tau_o)} d\lambda} \right| \quad (A.1)$$

where

$$C = [(\tau/\tau_o + \mu_r)^2 - (\tau/\tau_o - \mu_r)^2 \varepsilon^{-2t\tau}]^{-1}$$

$$\tau = (\lambda^2 + \gamma^2)^{1/2}$$

$$\tau_o = (\lambda^2 + \gamma_o^2)^{1/2}$$

$$\gamma_o = \frac{j2\pi}{\lambda_{air}} = \text{free-space propagation factor}$$

$$\gamma = (j\omega\mu_o\mu_r\sigma)^{1/2} = \text{propagation constant in the shield (displacement currents are neglected)}$$

$$\tau_r = \frac{|\gamma|}{\sqrt{2}} = (\omega\mu_o\mu_r\sigma/2)^{1/2} = \frac{1}{\delta}$$

$$\delta = (2/\omega\mu_o\mu_r\sigma)^{1/2} = \text{skin depth in the shield}$$

μ_r = relative permeability of the shield

t = shield thickness

σ = shield conductivity

$z = r_1 + r_2$ = center-to-center separation of the two loops

$J_1(\lambda a)$ = Bessel function of order one and argument (λa).

a = loop radius

λ = dummy variable of integration

$$r = \sqrt{a^2 + z^2}$$

λ_{air} = wavelength in air

Simplified approximate forms of Moser's formula can be derived under certain conditions [3, 4]. Let $r' = [a^2 + (z - t)^2]^{1/2}$ be termed the measurement distance. Then for conditions such that $r' < \frac{\lambda_{air}}{20}$, $\tau_r t > 2$, $\tau_r r' > 10$ and $\frac{\tau_r r'}{\mu_r} > 10$ are satisfied, the shielding equation takes on the much simpler form given below.

$$S.\ E._{dB} \simeq 8.686\ \sqrt{2}\tau_r t + 20\ \log_{10}\left|\left(\frac{\tau_r r'}{8.485\mu_r}\right)\left(\frac{r'}{z-t}\right)\left(\frac{r'}{r}\right)^3\right| . \qquad (A.2)$$

If, as is usually the case, $z \gg t$, then:

$$S.\ E._{dB} \simeq 8.686\sqrt{2}\tau_r t + 20\ \log_{10}\left|\frac{\tau_r z}{8.485\mu_r}\left(\frac{r}{z}\right)^2\right| . \qquad (A.3)$$

If in addition $z \gg a$, then:

$$S.E._{dB} \simeq 8.686\sqrt{2}\tau_r t + 20\ \log_{10}\left(\frac{\tau_r z}{8.485\mu_r}\right) . \qquad (A.4)$$

MISSION
of
Rome Air Development Center

RADC plans and executes research, development, test and selected acquisition programs in support of Command, Control Communications and Intelligence (C^3I) activities. Technical and engineering support within areas of technical competence is provided to ESD Program Offices (POs) and other ESD elements. The principal technical mission areas are communications, electromagnetic guidance and control, surveillance of ground and aerospace objects, intelligence data collection and handling, information system technology, ionospheric propagation, solid state sciences, microwave physics and electronic reliability, maintainability and compatibility.

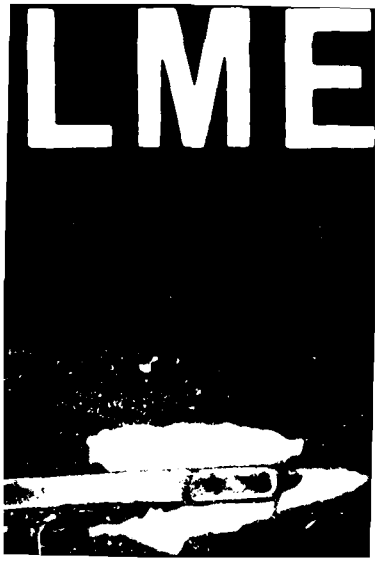
LME